

QUANTUM CHAOS, TRANSPORT, AND CONTROL—IN QUANTUM OPTICS*

JAVIER MADROÑERO^{1,2}, ALEXEY PONOMAREV²,
ANDRÉ R.R. CARVALHO², SANDRO WIMBERGER³, CARLOS VIVIESCAS²,
ANDREY KOLOVSKY², KLAUS HORNBERGER⁴, PETER SCHLAGHECK⁵,
ANDREAS KRUG^{2,†} and ANDREAS BUCHLEITNER²

¹Physik Department, Technische Universität München, James-Frank-Straße, D-85747 Garching, Germany

²Max-Planck-Institut für Physik komplexer Systeme, Nöthnitzer Str. 38, D-01187 Dresden, Germany

³Dipartimento di Fisica Enrico Fermi and CNR-INFM, Università di Pisa, Largo Pontecorvo 3, I-56127 Pisa, Italy

⁴Arnold-Sommerfeld-Zentrum für Theoretische Physik, Ludwig-Maximilians-Universität München, Theresienstr. 37, D-80333 München, Germany

⁵Theoretische Physik, Universität Regensburg, D-93040 Regensburg, Germany

1. Introduction	34
2. Spectral Properties	34
2.1. Parametric Level Dynamics and Universal Statistics	35
2.2. Spectral Signatures of Mixed, Regular-Chaotic Phase Space Structure	40
3. Dynamics and Transport	41
3.1. Atomic Conductance Fluctuations	42
3.2. Web-Assisted Transport in the Kicked Harmonic Oscillator	46
3.3. Ericson Fluctuations in Atomic Photo Cross Sections	49
3.4. Photonic Transport in Chaotic Cavities and Disordered Media	51
3.5. Directed Atomic Transport Due to Interaction-Induced Quantum Chaos	55
4. Control through Chaos	59
4.1. Nondispersive Wave Packets in One Particle Dynamics	61
4.2. Nondispersive Wave Packets in the Three Body Coulomb Problem	63
4.3. Quantum Resonances in the Dynamics of Kicked Cold Atoms	66
5. Conclusion	67
6. References	68

* We dedicate this paper to Herbert Walther, at the occasion of his 70th anniversary, in reverence to his contributions to the foundations of quantum optics, as well as to identifying the “quantum signatures of chaos” in the lab. Happy birthday!

† Present address: Siemens Medical Solutions, Erlangen, Germany.

Abstract

Chaos implies unpredictability, fluctuations, and the need for statistical modelling. Quantum optics has developed into one of the most advanced subdisciplines of modern physics in terms of the control of matter on a microscopic scale, and, in particular, of isolated, single quantum objects. *Prima facie*, both fields therefore appear rather distant in philosophy and outset. However, as we shall discuss in the present review, chaos, and, more specifically, quantum chaos opens up novel perspectives for our understanding of the dynamics of increasingly complex quantum systems, and of ultimate quantum control by tailoring complexity.

1. Introduction

Quantum optics has nowadays largely accomplished its strictly reductionist program of preparing, isolating and manipulating single quantum objects—atoms, ions, molecules, or photons—such as to access the very fundamentals of quantum theory, from quantum jumps [2,3] over the measurement process [4] and decoherence [5], to quantum nonlocality and entanglement [6], in the laboratory. The field turns “complex” now, by building up—or “engineering”—complexity from the bottom, with nonlinear Hamiltonian dynamics [7], particle–particle interactions [8,9], disorder [10] or noise [11,12] as essential ingredients. Somewhat unexpectedly, quantum optics therefore makes contact with quantum chaos—the theory of finite size, strongly coupled quantum systems.

While for a long time under the suspicion of rather mathematical interest, coming up with “large fluctuations and hazardous speculations”, quantum chaos [1] now finds an ever expanding realm of experimental applications [7,13–30]. In addition, it provides novel tools for the understanding and the robust control [14, 28,29,31,32] of the dynamics of increasingly “complex” quantum systems. In the present review, we recollect some of the generic features encountered within such “chaotic” quantum systems, and spell out their potential for the control of quantum dynamics in light-matter interaction.

2. Spectral Properties

There are different ways to approach quantum chaos. Possibly the most suggestive one proceeds along the semiclassical line, juxtaposing classical phase space structures or dynamics on the one side, and the quantum spectral density or wave function evolution in phase space, on the other [33–35]. The specific motivation of this program lies in the intricate nature of the semiclassical limit (“ $\hbar \rightarrow 0$ ”,

meaning the vanishing of Planck’s quantum when compared to typical classical actions on macroscopic scales), and, hence, of the emergence of classical from quantum dynamics at sufficiently large actions. This is an extremely attractive approach, with a beautiful mathematical and theoretical machinery, leading to important practical consequences, such as the rather recent semiclassical elucidation of the helium spectrum [36–41]. However, it is—by construction—bound to quantum systems with a well-defined classical counterpart, since it derives quantum features from the backbone of the underlying classical dynamics.

While we shall adopt the semiclassical perspective for the motivation or interpretation of some of the results to be discussed in this paper, we will often deal with systems which lack a well-defined classical analog. Therefore, most of our observations will be derived directly from the quantum spectrum of the specific systems under study.

2.1. PARAMETRIC LEVEL DYNAMICS AND UNIVERSAL STATISTICS

On the spectral level, quantum chaos is tantamount to the destruction of good quantum numbers [42,43]. Since the latter express symmetries, or dynamical invariants, of the specific system under study, quantum chaos occurs when these symmetries are destroyed, e.g., by the nonperturbative coupling of initially separable degrees of freedom. If a well-defined classical Hamiltonian dynamics underlies the quantum dynamics, good quantum numbers are inherited from the classical constants of the motion, and their destruction is paralleled by the invasion of classical phase space by chaotic motion.

Good quantum numbers can be considered, in a bounded system with a discrete spectrum, as the labels attributed to individual eigenvalues of the Hamiltonian. Symbolically, we may write for a system with three degrees of freedom:

$$H^{(\lambda)}|n \ell m\rangle^{(\lambda)} = E_{n \ell m}^{(\lambda)}|n \ell m\rangle^{(\lambda)}. \quad (1)$$

These labels are *good* labels in the sense that, if $H^{(\lambda)}$ depends parametrically on a real scalar λ , the eigenvectors $|n \ell m\rangle^{(\lambda)}$ do not (ex)change their specific character over a *finite* interval of λ .

The corresponding good quantum numbers lose their significance for the identification of individual eigenstates as soon as different eigenstates of $H^{(\lambda)}$ are strongly mixed by a perturbation which couples at least two of the degrees of freedom represented by the quantum numbers n , ℓ , and m , on *arbitrarily small* intervals of λ —they are “destroyed” by the perturbation-induced coupling.

In the jargon of quantum chaos, the parametric evolution of the eigenvalues $E^{(\lambda)}$ of some Hamiltonian $H^{(\lambda)}$ parametrized by the real scalar λ is called “regular level dynamics” if completely classifiable by good quantum numbers. “Chaotic” or “irregular level dynamics” (also “level spaghetti”) is encountered

when all good quantum numbers are destroyed. Such irregular level dynamics *alone* is one possible indicator of quantum chaos, without any recourse to some analogous classical dynamics.¹

A nice illustration of the transition from regular to irregular level dynamics is provided by the Floquet–Bloch spectrum generated by the Bose–Hubbard Hamiltonian under static tilt,

$$H_B = -\frac{J}{2} \left(\sum_{l=1}^L \hat{a}_{l+1}^\dagger \hat{a}_l + \text{h.c.} \right) + F \sum_{l=1}^L dl \hat{n}_l + \frac{W}{2} \sum_{l=1}^L \hat{n}_l (\hat{n}_l - 1). \quad (2)$$

The Hamiltonian is formulated in terms of the creation and annihilation operators \hat{a}_l^\dagger and \hat{a}_l of a bosonic atom at the lattice site l , with the associated number operators \hat{n}_l . It describes the dynamics of N ultracold bosonic atoms in a one-dimensional optical lattice of length L and lattice constant d . The implicit single band approximation assumes that no excitations to the first conduction band of the lattice can be mediated by the tilt, $Fd \ll \Delta E_{\text{gap}}$, nor by thermal activation, $kT \ll \Delta E_{\text{gap}}$, with ΔE_{gap} the band gap. J and W quantify the strength of the nearest neighbor tunneling coupling J , and of the on-site interaction strength W between the atoms, respectively, which compete with a static forcing of strength F . A suitable gauge transform reestablishes the translational invariance in space apparently broken by the static field term in (2), and additionally introduces an explicit, periodic time dependence with the Bloch period $T_B = 1/F$ [44]. The time evolution operator for one Bloch cycle in this time dependent coordinate frame is the Floquet–Bloch operator associated with H_B .

Figure 1 displays the level dynamics of the one cycle propagator, parametrized by F , for different values of the ratio of tunneling coupling to interaction strength. Clearly, when J and W become comparable, the eigenstates of the Floquet–Bloch operator interact strongly for any value of F , while in the limit $W \gg J$ (and equally so for $J \gg W$) individual eigenstates are clearly identifiable over large intervals of F . In this specific model—which is actually realized in laboratory experiments which load Bose Einstein condensates (BEC’s) into periodic optical lattices [8,45]—the transition from regular dynamics to quantum chaos is apparent and unambiguous. Yet, this interacting multiparticle system has no well-defined classical counterpart! Further down in this review (see Section 3.5), we will analyze the dynamical (and experimentally highly relevant) consequences of this transition. At present, it is enough to state that the qualitative transition observed in Fig. 1 is actually qualitatively underpinned by the cumulative spacing

¹ The term “dynamics” is motivated by considering the parameter λ as some generalized time, with the eigenvalues $E^{(\lambda)}$ some generalized particle position evolving under variations of λ .

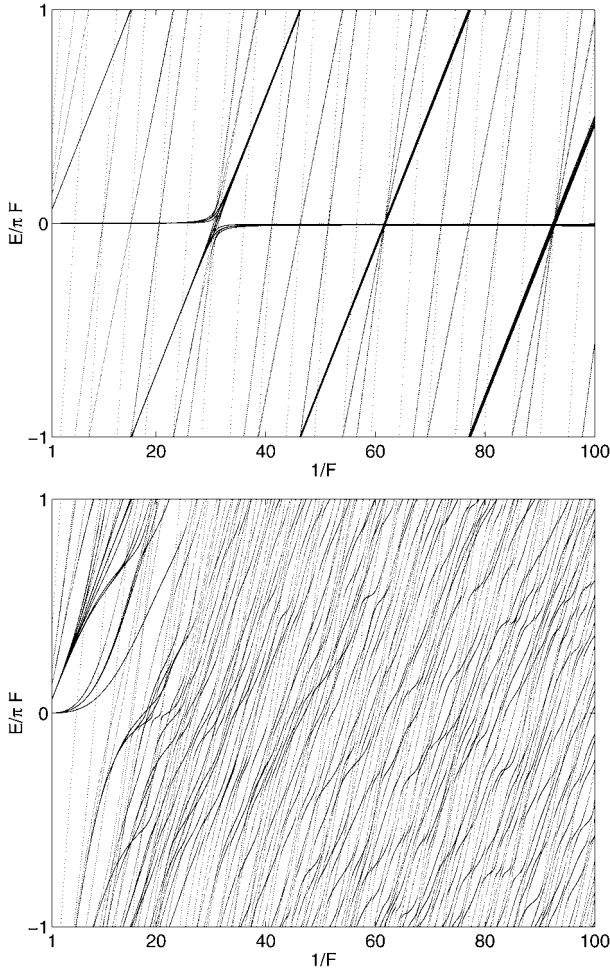


FIG. 1. Spectrum of the Floquet–Bloch operator generated by H_B as defined in (2), as a function of $1/F$, for $N = 4$ particles distributed over a lattice with $L = 7$ wells (periodic boundary conditions). Only states with quasimomentum $\kappa = 0$ are shown, in order to separate different symmetry classes [44]. The particle–particle interaction strength and the tunneling coupling are set equal to $W = 0.032$, and $J = 0.00076$ (top) and $J = 0.038$ (bottom), respectively. As we tune the tunneling coupling to a value comparable to the interaction strength, the “individuality” of the energy levels drowns in an irregular pattern: isolated avoided crossings between different energy levels which can be labeled by the interaction energy between the different particles of a given multiparticle eigenstate in the lattice [44] (for weak tunneling coupling, the distribution of the particles over the lattice characterizes a given eigenstate very well, except for resonant tunneling enhancements at isolated values of F) are replaced by strongly interacting levels, for arbitrary values of F .

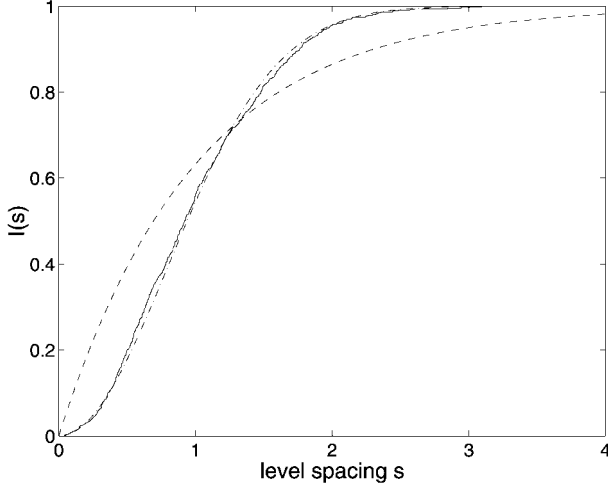


FIG. 2. Cumulative level spacing distribution of the Floquet–Bloch operator generated by H_B (Eq. (2)), for $N = 7$ bosonic atoms distributed over a lattice of length $L = 9$ (periodic boundary conditions), static tilt $F = 0.01$, tunneling strength $J = 0.038$, interaction strength $W = 0.032$ (full line). The statistics is obtained from the unfolded spectrum [43] with the symmetry class defined by quasimomentum $\kappa = 0$ [44]. The dashed and dash-dotted line indicate the RMT prediction for Poissonian and Wigner–Dyson statistics, respectively.

distribution,

$$I(s) = \int_0^s P(s') ds', \quad (3)$$

with $P(s)$ the probability distribution of the (normalized and unfolded, see, e.g., [43]) spacings s between adjacent eigenphases of the Floquet–Bloch operator [44]. Inspection of Fig. 2 clearly shows that $I(s)$ (and equally so $P(s)$), but the comparison of $I(s)$ with the random matrix prediction is known to be more reliable, in particular in the vicinity of $s = 0$) exhibits Poissonian statistics, $P(s) = \exp(-s)$, in the regular limit, and Wigner–Dyson statistics, $P(s) = \pi s \exp(-\frac{\pi}{4}s^2)/2$, in the chaotic limit (more precisely, the level spacings faithfully reproduce the COE statistics of random matrices of the circular (C) orthogonal (O) ensemble (E) [46]). Hence, by simply tuning the ratio of J and W , in the perfectly deterministic Hamiltonian (2), we induce a spectral structure which enforces a statistical description if we seek for a robust, quantitative description of the system dynamics.

Another example of chaotic level dynamics is shown in Fig. 3, where we display the parametric evolution of the eigenphases of the Floquet operator of the kicked harmonic oscillator. The Floquet operator—or one cycle propagator— $U = \exp(-i \int_0^\tau H(t') dt'/\hbar)$, with τ the kicking period, is generated by the

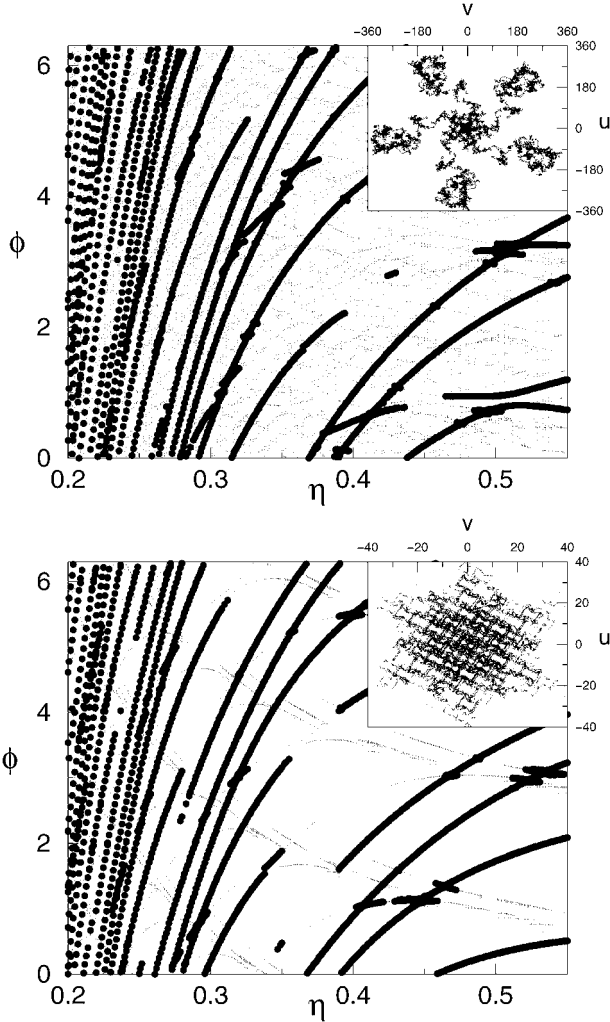


FIG. 3. Spectrum of the Floquet operator generated by H_{kho} in (4), as a function of the Lamb–Dicke parameter η , for a fixed phase space structure indicated by the single trajectory runs over 40,000 kicks in the insets (u and v are suitably defined, canonical phase space variables, see [32]). Only eigenphases with an overlap larger than 10^{-3} with the initial state $|\psi_0\rangle$ are represented. Filled circles represent $|\psi_0\rangle = |0\rangle$, while dots refer to a displaced vacuum centered at (1.3, 3.0) (top) and (1.2, 2.0) (bottom).

Hamiltonian

$$H_{\text{kho}} = \hbar v \hat{a}^\dagger \hat{a} + K \frac{mv}{k^2} \left\{ \cos[\eta(\hat{a} + \hat{a}^\dagger)] \right\} \sum_{n=0}^{\infty} \delta(t - n\tau). \quad (4)$$

This is a paradigmatic example of a quantum chaotic system which, on the classical level, does *not* obey the Kolmogorov–Arnold–Moser (KAM) theorem (which guarantees stability with respect to small perturbations) [47], due to the degeneracy of the unperturbed spectrum of the harmonic oscillator. In (4), \hat{a} and \hat{a}^\dagger represent the annihilation and creation operators of the harmonic oscillator modes of the translational degree of freedom (for a particle of mass m), and K measures the strength of the kicking mediated by the periodically flashed standing wave potential with wave vector k . $\eta = k\sqrt{\hbar/2m\nu}$ is the experimentally easily tunable Lamb–Dicke parameter, which essentially measures the ratio of the width of the harmonic oscillator ground state in units of the wave length of the kicking potential.

H_{kho} can be realized in semiconductor heterostructures [48] as well as with cold, harmonically trapped ions, and allows for unlimited, superdiffusive energy growth (i.e., for trapped ions, unlimited heating) under rather precisely defined conditions, as we will see further down in this review. This specific dynamical behavior has once again its root in the largely irregular level dynamics shown in Fig. 3, which is here illustrated for two different ratios $q = 2\pi/\tau\nu = 5$ (top) and $q = 6$ (bottom) of kicking period τ and oscillator period $1/\nu$, under variation of η . These two choices correspond to a crystalline and quasicrystal [49] symmetry of the classical phase space structure, as indicated by the classical sample trajectories shown in the corresponding insets. The crystal case still bears some remnants of regularity, with regularly aligned avoided crossings coexisting with apparently randomly distributed anticrossings of variable size. The quasicrystal case, in contrast, exhibits an extremely complicated level structure, with no apparent regularity left. The details and structure of the level dynamics remain to be understood, but part of its peculiarities can already be exploited for novel perspectives of quantum control, as we shall see further down in Section 3.2.

2.2. SPECTRAL SIGNATURES OF MIXED, REGULAR-CHAOTIC PHASE SPACE STRUCTURE

In quantum systems with a well-defined classical analog which exhibits mixed regular chaotic phase space structure [21,31,36,50–62], the parametric evolution of the eigenenergies does not exhibit an unambiguously “chaotic” structure. Eigenenergies associated with eigenstates that are localized in phase space domains of regular motion are only weakly affected by the adjacent chaotic phase space component and evolve, in general, smoothly under variations of some control parameter λ . Since regular domains of phase space are associated with local dynamical invariants, these states can actually be labeled with good quantum numbers, and undergo, in general, only locally avoided crossings with states living on the chaotic phase space component. Consequently, such states “go straight” in

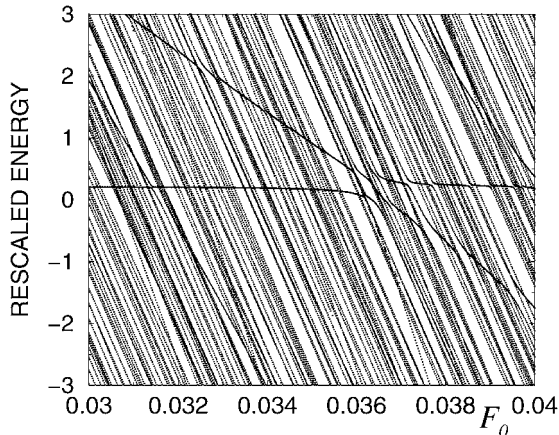


FIG. 4. Parametric evolution of the spectrum of a microwave driven hydrogen atom, in suitably rescaled energy units, under variation of the driving field amplitude F_0 (measured in units of the Coulomb field experienced by the Rydberg electron propagating along an unperturbed Kepler orbit with principal quantum number n_0) [31]. Two energy levels, which anticross at $F_0 \simeq 0.036$, clearly “go straight” in this plot, and only weakly interact with the “level spaghetti” background: They represent eigenstates of the atom in the field which are localized on elliptic regions in the classically mixed regular-chaotic phase space, and are therefore shielded against strong interaction with states living in the chaotic phase space component.

the energy level dynamics, with almost constant slope, as displayed in Fig. 4 for the (quasi)energy level associated with a wave packet eigenstate of a microwave-driven Rydberg state of atomic hydrogen (see also Section 4.1 below). In a rather abstract sense, such states can therefore sometimes be attributed solitonic character [63]—they anticross with “chaotic” eigenstates without changing their characteristic features like localization properties, dipole moments, or the like. Conversely, the soliton-like motion under variations of λ can serve as an identifier for eigenstates which are shielded from the irregular part of the spectrum, even in the absence of an unambiguous classical dynamics—examples are found, e.g., in microwave driven Rydberg states of alkali atoms [64], with their nonhydrogenic multielectron core which induces quantum mechanical diffraction effects on top of the semiclassical Rydberg dynamics [57,65].

3. Dynamics and Transport

The specific spectral structure of a given quantum system fully determines the associated time evolution. If we initially prepare our system in the state $|\psi_0\rangle$, the

action of the time evolution operator is given by

$$U(t)|\psi_0\rangle = \sum_n \exp(-iE_n t/\hbar) |E_n\rangle \langle E_n|\psi_0\rangle, \quad (5)$$

where we assume, for simplicity, a discrete spectrum $\{E_n\}$ of H . Alternatively, the energies E_n may be thought of as complex eigenvalues $E_n - i\Gamma_n/2$ of some effective Hamiltonian, with the decay rates Γ_n representing, for instance, the nonvanishing coupling to a continuous part of the spectrum [66–69]. In most experiments, some sort of (auto)correlation signal like

$$\begin{aligned} C(t) &= \langle \psi_0|U(t)|\psi_0\rangle = \sum_n |\langle \psi_0|\phi_n\rangle|^2 \exp(-iE_n t/\hbar) \\ &\rightarrow \sum_n |\langle \psi_0|\phi_n\rangle|^2 \exp(-iE_n t/\hbar) \exp\left(-\frac{\Gamma_n}{2}t\right) \end{aligned} \quad (6)$$

is measured [70,71], which, besides the purely spectral ingredients E_n and Γ_n also includes a local “probe” $|\langle \psi_0|\phi_n\rangle|^2$ of the spectrum, in the vicinity of the state $|\psi_0\rangle$ with which the time evolved wave function is to be correlated. Also ionization or survival probabilities which are often encountered in atomic ionization experiments or in model systems which probe quantum mechanical phase space transport are closely related to such correlation functions, possibly amended by an additional summation over a (discrete or continuous) set of “test functions” $|\psi_0\rangle$ [53,72–75].

3.1. ATOMIC CONDUCTANCE FLUCTUATIONS

It is immediately clear from the form of (6) that the dynamics of a chaotic quantum system in the sense of chaotic level dynamics as illustrated in Section 2 will exhibit a sensitive parameter dependence, reflecting the parametric evolution of the spectrum. A nice example is provided by the ionization yield of one electron Rydberg states under microwave driving—which probes the asymptotic electron transport induced by the external perturbation. In such type of experiments [21, 50,76–88], one electron Rydberg states (with excitations to principal quantum numbers around $n_0 \simeq 70$) are exposed to a microwave field of frequency ω and amplitude F , for an adjustable interaction time t . The experimentally easily accessible ionization yield P_{ion} is formally given [73] by

$$P_{\text{ion}} = 1 - \sum_j |\langle \psi_0|\phi_j\rangle|^2 \exp(-\Gamma_j t). \quad (7)$$

The sum extends over the complete spectrum of the atom dressed by the field, though weighted by the overlap of the (field free) initial state with the atomic

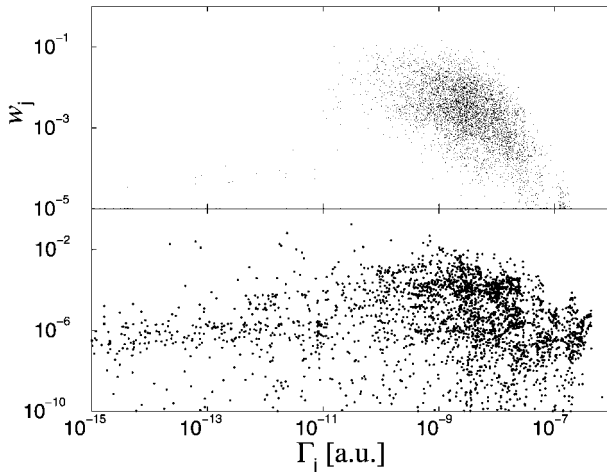


FIG. 5. Typical distribution of the ionization rates Γ_j and local weights $\mathcal{W}_j = |\langle \psi_0 | \phi_j \rangle|^2$ entering the expression (7) for the ionization yield P_{ion} of an atomic Rydberg state under electromagnetic driving. In the upper plot, 500 spectra of a one-dimensional model atom initially prepared in the Rydberg state $|n_0 = 100\rangle$ are accumulated, for driving field frequencies $\omega/2\pi = 13.16 \dots 16.45$ GHz, at fixed photonic localization length $\ell = 1$ (see Eq. (9)). In the lower plot, one single spectrum of the three-dimensional hydrogen atom initially prepared in the state $|n_0 = 70 \ell_0 = 0 m_0 = 0\rangle$, at $\omega/2\pi = 35.6$ GHz and $\ell = 1$ is shown. There is no apparent correlation between ionization rates and local weights—which also manifests in the parameter dependence of P_{ion} itself, see Fig. 6.

dressed states for the specific choice of ω and F . Typically, several hundreds to thousands dressed states contribute to the representation of $|\psi_0\rangle$ [89,90].

Under changes of ω or F , not only the decay rates Γ_j of the individual dressed states will fluctuate, but, equally important, the local weights $|\langle \psi_0 | \phi_j \rangle|^2$ —as a corollary of the destruction of good quantum numbers in the realm of quantum chaos: The characteristic properties of the system eigenstates vary rapidly with the control parameter (here ω or F), and so does the decomposition of the (parameter-independent) initial state $|\psi_0\rangle$. In general, the fluctuations of decay rates and overlaps are uncorrelated, as illustrated in Fig. 5, for typical driving frequencies and amplitudes, and for a one-dimensional model of the driven atom, as well as for the real, three-dimensional system. While one might believe that these fluctuations average out under the summation in (7), this is actually not the case—Fig. 6 shows the ionization yield of atomic hydrogen, initially prepared in the unperturbed $n_0 = 100$ Rydberg state, under microwave driving with variable frequency. Indeed, P_{ion} fluctuates rapidly with the scaled frequency $\omega_0 = \omega \times n_0^3$ [93] in this plot, at fixed n_0 . This is the dynamical manifestation of the sensitive ω_0 -dependence of the quantities which determine P_{ion} , according to (7). While this sensitive dependence shows that the mere ionization yield for

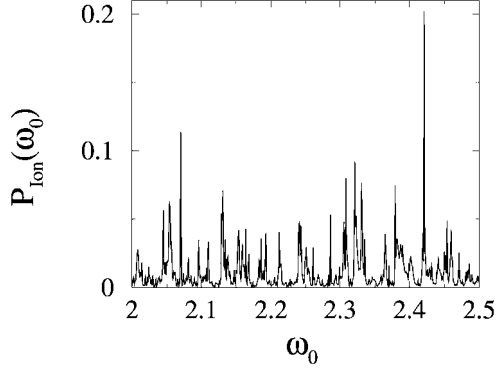


FIG. 6. Ionization yield P_{ion} , Eq. (7), of a one-dimensional Rydberg atom launched in the Rydberg state $|n_0 = 100\rangle$, as a function of the scaled driving field frequency $\omega_0 = \omega \times n_0^3$, at fixed localization length $\ell = 1$ (see Eq. (9)). The strong fluctuations of the signal under variations of ω_0 are characteristic of a strongly localized (in the sense of Anderson [91]) transport process (here on the energy scale, and induced by the external driving) in disordered media [92].

given ω and F does not provide a robust characterization of the electronic transport process induced by the external drive, a statistical analysis allows for some insight: The atomic conductance [94]

$$g_{\text{atom}} = \frac{1}{\Delta} \sum_j |\langle \psi_0 | \phi_j \rangle|^2 \Gamma_j, \quad (8)$$

formally equivalent to the time derivative of the ionization yield at $t = 0$ (with Δ the average spacing between adjacent energy levels), exhibits a log-normal distribution, i.e., $\ln g_{\text{atom}}$ is normally distributed, when sampled for a fixed *photonic localization length* [95]

$$\ell = \frac{\Delta E}{\omega} = \frac{6.66 F_0^2 n_0}{\omega_0^{7/3}} \left(1 - \frac{n_0^2}{n_c^2}\right)^{-1}. \quad (9)$$

The latter is a measure of the typical decay length of the electronic population distribution over the near resonantly coupled Rydberg states away from the atomic initial state $|\psi_0\rangle$, and determines the asymptotic continuum transport *on average*, according to [93]:

$$\langle \ln g_{\text{atom}} \rangle \sim 1/\ell. \quad (10)$$

In particular, this proportionality relation together with the lognormal distribution for fixed localization length, which are established in Figs. 7 and 8 for a one-dimensional hydrogen atom (which is a reliable model for the description of real 3D hydrogen under external microwave driving, when initially prepared in

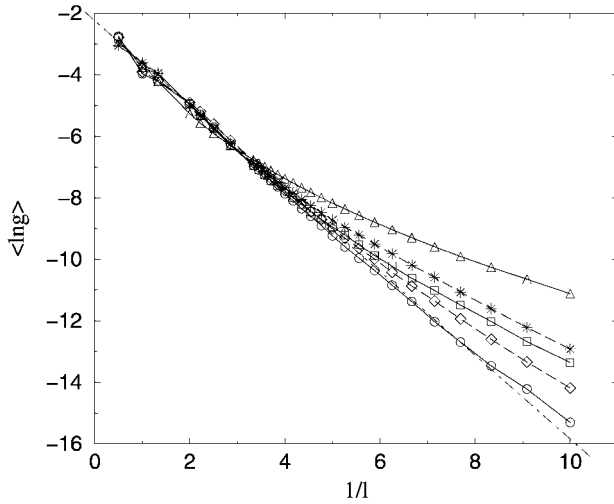


FIG. 7. Average value of the natural logarithm of the atomic conductance g vs. the inverse photonic localization length $1/\ell$, for a one-dimensional Rydberg atom initially prepared in the state $|n_0\rangle$ with principal quantum number $n_0 = 40, 60, 70, 90, 100$ (from top to bottom). Clearly, the direct proportionality (10) predicted by the Anderson picture is very well satisfied for sufficiently large values of n_0 [93].

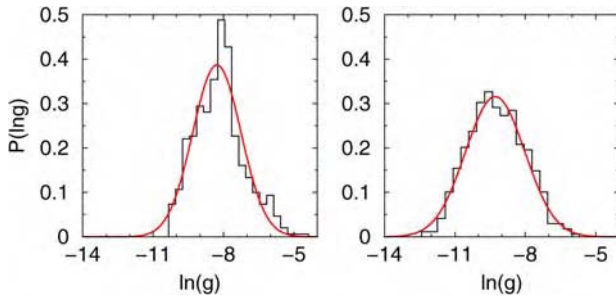


FIG. 8. Distribution (histograms) of the atomic conductance g of a one-dimensional Rydberg atom [93,94,97], sampled over 500 different spectra with photonic localization length $\ell = 0.2$, in the frequency range $\omega_0 = 2.0 \dots 2.5$, for initial principal quantum number $n_0 = 40$ (left) and $n_0 = 100$ (right). The log-normal fit is excellent for $n_0 = 100$, in perfect quantitative agreement with the Anderson picture. Finite size effects lead to discrepancies between the numerical distribution of $\ln g$ and the lognormal fit at lower excitations around $n_0 = 40$.

an extremal parabolic state [96,97]), provide strong quantitative support for the analogy between electronic transport along the energy axis in periodically driven atomic Rydberg states and electronic transport across one-dimensional disordered

wires [92,94,98–100]: *Destructive* quantum interference of the many transition amplitudes connecting the initial atomic state to the atomic continuum, in the atomic problem, and the left and the right edge of the disordered wire, in the mesoscopic problem, leads to an exponential suppression of the quantum transport, as opposed to diffusive transport in a classical description. This phenomenon is known as *Anderson localization* [91,101–104] (also *strong localization*), and was baptized *dynamical localization* [17,19,105–115] in the realm of quantum chaos, where dynamical chaos substitutes for disorder.

3.2. WEB-ASSISTED TRANSPORT IN THE KICKED HARMONIC OSCILLATOR

An alternative scenario for the detection of chaos-induced fluctuations on the level of quantum transport properties is provided by cold, harmonically trapped ions under periodic kicking. We already have seen in Section 2.1 that the energy level dynamics of the kicked harmonic oscillator which is realized in such a setting exhibits many avoided crossings of variable size. Indeed, if we launch a wave packet in the harmonic oscillator ground state and monitor its mean energy as time evolves, the energy growth rate is found to depend sensitively on the precise value of the Lamb–Dicke parameter η , which is easily tuned in state of the art ion trap experiments. Figure 9 shows such behavior, for three different values of η , at fixed classical phase space structure ($\eta \sim \sqrt{\hbar}$ determines the effective size of \hbar with respect to the typical classical action of the harmonic oscillator; also see Fig. 3). Correspondingly, the mean energy extracted by the atoms from the kicking field, after a fixed interaction time, exhibits strong, apparently random fluctuations with the Lamb–Dicke parameter, as illustrated in Fig. 10. Once again, this can be directly associated with the avoided crossings in the energy level diagram in Fig. 3, and is strongly reminiscent of the atomic conductance fluctuations encountered in Fig. 6. Note, however, that the classical phase space structure of the kicked harmonic oscillator is different from the phase space structure of the harmonically driven Rydberg atom, since we are here dealing with a non-KAM system. The signature of this non-KAM structure in the spectral statistics is hitherto unexplored, and represents a formidable challenge, both for random matrix theory, as well as for computational physics.

We can nonetheless precisely identify the universal cause of the locally enhanced energy absorption of the trapped ions from the kicking field, by inspection of the eigenstates which undergo the specific avoided crossing, at a given value of η : Fig. 11 shows the Husimi phase space projections [69] of those eigenfunctions which account for the dominant part in the decomposition of the ionic initial state $|\psi_0\rangle = |0\rangle$ in the vicinity of $\eta = 0.464$ (the associated level anticrossing is shown by the inset in Fig. 9), i.e., at a value where strongly enhanced heating of the ions is observed. While for Lamb–Dicke parameters slightly below and

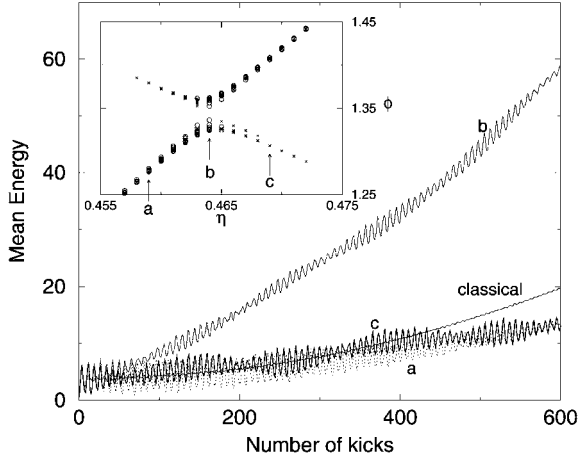


FIG. 9. Mean energy of the kicked harmonic oscillator, Eq. (4), for crystal symmetry, $q = 6$, kicking strength $K = 2.0$, and initial state $|\psi_0\rangle = |0\rangle$. Tiny changes of the Lamb–Dicke parameter from $\eta = 0.459$ (a) over $\eta = 0.464$ (b) to $\eta = 0.469$ (c) lead to a locally dramatic enhancement of the energy absorption by the trapped particle from the kicking field, with respect to the classical heating process. This local enhancement can actually be traced back to an avoided crossing of the continuation of the eigenphase associated with $|\psi_0\rangle$ in the level dynamics (inset) with a “web-state” (see Fig. 11) reaching far out to high energies in the harmonic oscillator phase space. The above values of η are indicated by the corresponding labels, in the inset. Filled black circles indicate an overlap of more than 1% of the associated eigenstate with the initial state $|\psi_0\rangle$.

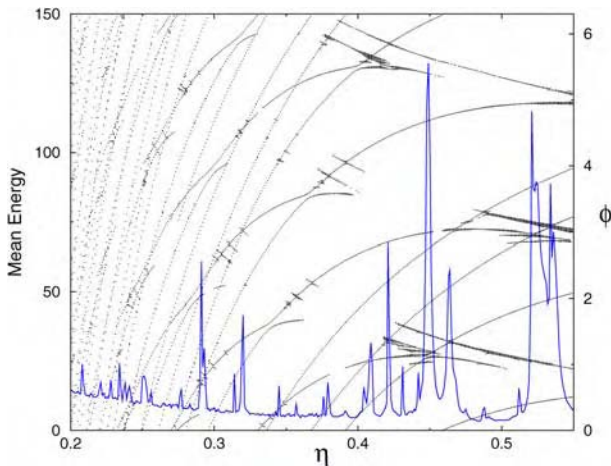


FIG. 10. Mean energy (left vertical axis) after 600 (full line) kicks vs. the Lamb–Dicke parameter η . The classical phase space structure is fixed by $K = 2.0$ and $q = 6$. Locally strongly enhanced energy absorption can always be traced back to avoided crossings of the initial state with web states, as apparent from the underlaid energy level dynamics (right vertical axis).

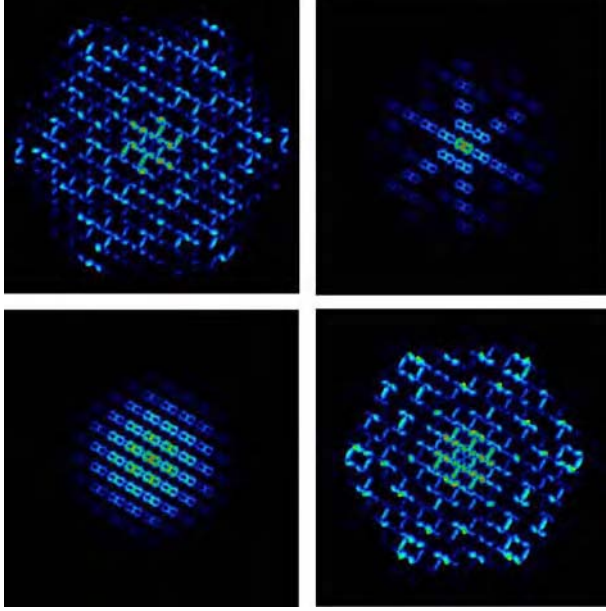


FIG. 11. Husimi representations of the eigenstates associated with the labels a (left column) and c (right column) in the inset of Fig. 9, in the rescaled phase space coordinates $v/2\eta = -60 \dots +60$ and $u/2\eta = -60 \dots +60$ of the insets of Fig. 3. The top left and bottom right plot represent web states associated with the top left and bottom right branch of the avoided crossing shown in the inset of Fig. 9. At $\eta = 0.464$, i.e., at the center of that avoided crossing, they strongly mix with the continuation (bottom left and top right branch of the avoided crossing, and bottom left and top right Husimi representation in the present figure) of $|\psi_0\rangle$, thus giving rise to efficient transport from the trap center to high energy states of the harmonic oscillator, along the stochastic web of the underlying classical phase space flow. Since the avoided crossing of the web state with the localized state occurs at fixed phase space structure, this is a pure quantum tunneling effect, without classical analog.

slightly above this critical value the eigenstate which is strongly localized in the vicinity of the origin of phase space has the largest weight in the initial state decomposition, an eigenstate localized on the stochastic web has equal weight right at $\eta = 0.464$. The existence of such web states is a peculiarity of non-KAM systems and is at the very origin of the observed enhanced energy growth, simply since the stochastic web reaches out to infinity, and therefore provides an efficient transport channel to high energy states of the oscillator. Since the avoided crossing which mediates the coupling of the initial state to the web state occurs under changes of the effective value of \hbar (via η), at fixed phase space structure, we have here—much as in the above case of strong localization in the ionization process of periodically driven atoms—a pure quantum effect without classical analog, leading now to a dramatic enhancement of the asymptotic transport, as

compared to the classical dynamics. A closely related phenomenon has been observed in the conductance across semiconductor superlattices, in the presence of a tunable magnetic field [48]. Since there the magnetic field allowed to switch between localized and delocalized (i.e., web-) states, web-states mediate, in some sense, metal-insulator like transitions.

3.3. ERICSON FLUCTUATIONS IN ATOMIC PHOTO CROSS SECTIONS

In the preceding two subsections, we encountered examples of a sensitive dependence of asymptotic transport on some control parameter, typical of quantum chaotic systems, in explicitly time dependent transport processes. As a third example, we now consider the continuum decay of Rydberg electrons induced by static external fields, which can be probed through the photoabsorption cross section for a probe laser beam from the atomic ground state into the Rydberg spectrum. Indeed, an atomic one electron Rydberg system exposed to perpendicularly oriented, static electric and magnetic fields, allows us to realize such a situation: The Hamiltonian reads

$$H_{\text{ExB}} = \frac{\mathbf{p}^2}{2} + V_{\text{atom}}(r) + \frac{B}{2}L_z + \frac{B^2}{8}(x^2 + y^2) + Fx, \quad (11)$$

in atomic units, with F and B the strength of the electric and magnetic field, respectively, and L_z the angular momentum projection on the magnetic field axis. If $V_{\text{atom}}(r)$ is given by the hydrogenic Coulomb potential, the diamagnetic term in (11) is known to induce chaotic motion in the bound space dynamics of the Rydberg electron. For $B = 0$ the electric field, while leaving the dynamics completely integrable, induces a Stark saddle and, hence, strong coupling of the bound eigenenergies with the continuum part of the spectrum. If both external fields are present, all symmetries of the unperturbed Coulomb problem are destroyed, and one faces a truly three-dimensional problem which exhibits dynamical chaos. In the case of alkali atoms, the additional presence of a multielectron core is not expected to suppress the signature of the classically chaotic Coulomb dynamics, on the spectral level [57,116,117].

Due to the suppression of the ionization threshold by the electric field, the high lying Rydberg states can acquire relatively large autoionization rates Γ_j , with an average value $\bar{\Gamma}$ which can become larger than the mean level spacing Δ of the (quasi)discrete energy levels E_j , i.e., $\bar{\Gamma} > \Delta$. In this regime of *overlapping resonances*, *Ericson fluctuations* [118–122] are expected in the photoabsorption cross section

$$\sigma(E) = \frac{4\pi(E - E_0)}{c\hbar} \text{Im} \sum_j \frac{|\langle g|T|E_j\rangle|^2}{E_j - i\Gamma_j/2 - E} \quad (12)$$

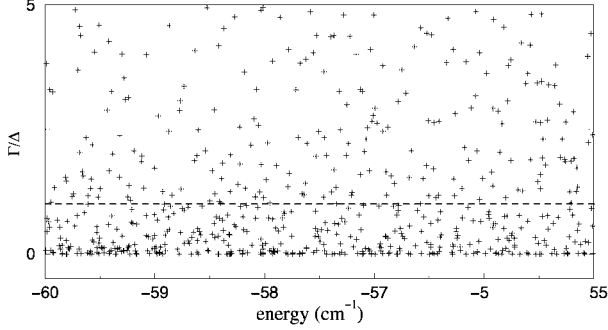


FIG. 12. Distribution of the resonance widths Γ_j which contribute to the photo cross section $\sigma(E)$, Eq. (12), in an energy interval which covers the experimentally [27,123] scanned region. The dashed line indicates the average (local) spacing Δ of the resonance states on the energy axis. Approx. 65% of them exhibit overlapping widths, $\Gamma_j > \Delta$.

from the atomic ground state $|g\rangle$ into the Rydberg regime at energy E : Bound-continuum transition amplitudes which mediate the decay of individual resonances couple to overlapping intervals of continuum states, and thus may interfere. Consequently, one expects interference structures in the cross section which can no more be attributed to individual resonance eigenstates with a specific width Γ_j , but are rather due to the interference of several decay channels, and exhibit typical widths *smaller* than $\bar{\Gamma}$. If a classical analog dynamics is available, these structures are predicted to be correlated on an energy scale which is determined by the dominant Lyapunov exponent of the classically chaotic dynamics, i.e., by the shortest decorrelation time scale of the classical dynamics [120].

Indeed, the transition into the Ericson regime has recently been observed in the photoionization cross section of rubidium Rydberg states in the presence of crossed fields [27,123]. A detailed theoretical analysis of the experimental situation shows that the laboratory results indeed entered the regime of overlapping resonances, and approx. 65% of all resonance eigenstates contributing to the photoabsorption signal have widths which are *larger* than the mean level spacing Δ . Figure 12 shows the numerically calculated distribution of resonance widths over the energy range probed by the experiment, under precisely equivalent conditions as in the experiment (fixed by the strength of the magnetic and electric fields). Besides the strongly fluctuating background signal, the cross section $\sigma(E)$ displayed in Fig. 13 also shows some narrow resonances on top, which stem from isolated resonances with $\Gamma_j < \Delta$. However, many of the structures with a width smaller than $\bar{\Gamma}$ can no more be associated with single isolated resonances, and thus indicate the interference of different decay amplitudes.

Thus, we observe the coexistence of individually resolved resonances with Ericson fluctuations. This it is not too surprising, since the original Ericson sce-

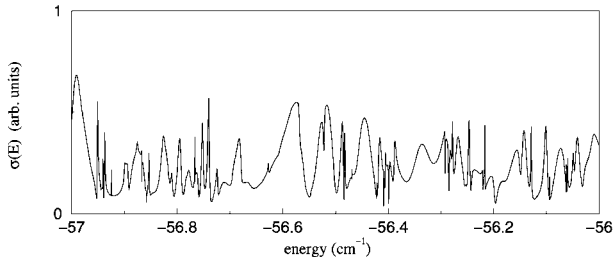


FIG. 13. Numerically obtained photo cross section (12) of rubidium Rydberg states in crossed electric and magnetic fields [124], deduced from a parameter free diagonalization of the Hamiltonian (11), using exactly the experimental parameters [27], $B = 2.0045$ T, $F = 22.4$ kV/m.

nario was inspired by highly excited compound nuclei with a large number of essentially equally weighted decay channels, while we are here dealing with a low-dimensional atomic decay problem, where different decay channels (e.g., through different angular momentum channels) have certainly different weights and equally different effective bound-continuum coupling constants.

Once again, due to the underlying chaotic level structure—here additionally complicated by resonance overlap—the experimentally accessible cross section shows erratic fluctuations, essentially uncorrelated on energy scales which are larger than the inverse of the characteristic life time of the ion–electron compound (which, in a classical picture, is determined by the largest Lyapunov exponent).

3.4. PHOTONIC TRANSPORT IN CHAOTIC CAVITIES AND DISORDERED MEDIA

In the previous section, we showed how the fine interplay between overlapping and isolated resonances determines the nature of the fluctuations in the transport properties of chaotic systems. In this section, we shall consider a novel kind of systems for which this interplay has also a determinative role: random lasers.

In contrast to standard lasers, random lasers do not possess mirrors. They are a class of nonlinear amplifiers realized in disordered dielectrics with a fluctuating dielectric constant that varies randomly in space. Light amplification is provided by an active optical medium, while the multiple chaotic scattering of photons in the random medium constitutes the feedback mechanism. Due to multiple scattering, the time spent by the light inside the active medium is enhanced. This, in turn, increases the probability of stimulated emission, making the field amplification efficient. Laser oscillations emerge when the radiation losses are overcome by the light amplification.

In recent years, several experiments on random lasers (see Ref. [125] for a review) as well as on lasers in chaotic resonators [126,127] have attracted considerable interest in the characterization of the properties of light emitted by these devices. Most striking are the generic signatures of the underlying disorder of the random media in the emission spectra: In samples with a low density of scatterers [128], light is only weakly confined and we expect the resonant modes to overlap. Once the pump energy exceeds the laser threshold, the onset of lasing is signaled by a collapse of the thermal emission spectrum into a single broad peak with a width of a few nanometers at the center of the amplification bandwidth. For samples with a high density of scatterers [128], on the other hand, some well-resolved resonant modes exist. As soon as the laser enters the operation regime above threshold, several very sharp peaks appear, the frequencies (within the amplification bandwidth) and strengths of which fluctuate strongly from sample to sample.

The above-mentioned features of the emission spectra cannot be explained by standard laser theory [129–131]. The reasons are twofold: First, in random lasers the spatial structure of the resonant modes as well as their frequencies depend on the statistical properties of the disordered medium. Random lasers, therefore, must be analyzed in an statistical fashion. Second, due to the absence of mirrors, light in random lasers is only weakly confined, giving rise to spectrally overlapping resonances. Recently, based on a field quantization method for open systems with large outcoupling losses [132–134], a quantum theory of random lasing incorporating both effects, random scattering of light and mode overlap, was proposed [135].

For a random laser with an active medium composed of two-levels atoms, the quantum Langevin equations of motion for the field variables are

$$\dot{a}_\lambda(t) = -i \sum_{\lambda'} \mathcal{H}_{\lambda\lambda'} a_{\lambda'}(t) + \sum_p g_{\lambda p}^* \sigma_{-p}(t) + F_\lambda(t). \quad (13)$$

Here, a_λ is the annihilation operator of the field mode λ , and σ_{-p} is the dipole operator of the p th atom. The coupling amplitudes $g_{\lambda p}$ between field and atoms are proportional to the atomic dipole d and to the field amplitude $u(\mathbf{r})$ at the position of the atom, $g_{\lambda p} \propto du_\lambda(\mathbf{r}_p)$. Equation (13) should be complemented with the equations of motion for the atomic operators, which we have omitted as they remain the same as those found in standard laser theory [129]. There are drastic differences between Eq. (13) and the independent-oscillator equations of standard laser theory. They arise from the fact that in order to account for the strong coupling of the field with the outside, all internal modes must now leak into the same external channels, i.e., they are coupled to the same bath. Hence, the internal dynamics of the field is determined by the non-Hermitian operator \mathcal{H} , accounting for the system's losses due to the coupling with the exterior, and coupling the different

modes a_λ . Additionally, and consistently with the fluctuation–dissipation theorem, the noise operators F_λ of the different modes are correlated, $\langle F_\lambda^\dagger F_{\lambda'} \rangle \neq \delta_{\lambda\lambda'}$ (the expectation value is defined with respect to the state of the bath).

The emission properties of random lasers are determined by the complex eigenvalues $\omega_k - i\Gamma_k/2$, and the nonorthogonal eigenfunctions $R(\mathbf{r})$ of \mathcal{H} . Due to the strong correlation among modes, the relation between the mean frequency separation Δ of the real frequencies ω_k , and the average decay rate $\bar{\Gamma}$ of the modes is of crucial relevance for the emission spectra. In the regime of overlapping resonances, $\bar{\Gamma} > \Delta$, typically many broad modes will contribute to the emitted radiation. The resulting spectrum is then a smooth function of the frequency. On the contrary, in the regime of isolated resonances, $\bar{\Gamma} < \Delta$, the spectrum consists of a set of sharp peaks located at the resonant frequencies of the system. More striking, however, is the effect of the mode correlations on the coherence time of the random laser emission. For single mode lasing the coherence time $\delta\tau$ is inversely proportional to the laser line width $\delta\omega$. The latter was first calculated for standard lasers by Schawlow and Townes [136], by taking into account the spontaneous emission noise, and was found to decrease for increasing output intensities, $\delta\omega_{\text{ST}} \sim 1/I$. In random lasers, however, the noise correlation between different modes leads to an enhancement of the line width. One then has [132]

$$\delta\omega = K\delta\omega_{\text{ST}}, \quad (14)$$

where $K \geq 1$ is the so called Petermann factor [137–139]. K can be related to the self-overlap of the nonorthogonal laser mode $R(\mathbf{r})$, and is a measure of the correlations in the system. Hence, the coherence time of a random laser is smaller than the coherence time of a standard laser with the same output intensity.

The signatures of the underlying disorder in random lasers are also present in the photon statistics of the emitted light. Though for light propagating in a disordered material the photon statistics below threshold is well understood [140,141], only recently the nonlinear optical regime above threshold has been investigated [142–145]. As an example, we evaluate the mean photocount of the emitted field from a chaotic laser resonator in the regime of single-mode lasing [142]. We consider the coupling of the cavity to the outside to be weak, so that all resonances in the cavity are well defined. In this perturbative limit, the non-Hermitian operator \mathcal{H} in Eq. (13) becomes diagonal, and the laser mode a decouples from all other modes. Moreover, since the cavity opening is small, we can replace $R(\mathbf{r})$ by the orthogonal close cavity modes $u(\mathbf{r})$. In chaotic resonators the amplitude $u(\mathbf{r})$ at a point \mathbf{r} behaves like a Gaussian random variable, and is uncorrelated with the amplitude at any other point, provided it lies further apart than an optical wave length λ [146,147]. As we shall show, these spatial fluctuations induce strong mode-to-mode fluctuations in the laser emission.

In its steady-state, the laser is characterized by three parameters comprising the effects of the active medium on the field: The linear gain A , the nonlinear

saturation B , and the total loss rate C . The photon number distribution giving the probability to find the laser field at a time t with n photons is [130]

$$P_n = \mathcal{N} \frac{(An_s/C)^{n+n_s}}{(n+n_s)!}, \quad (15)$$

where the symbol \mathcal{N} stands for a normalization constant, and the nonlinear saturation B enters through the so called saturation photon number $n_s = A/B$. When the number of atoms in the active medium is large, A and B are shown to acquire sharp values. $C = \Gamma + \kappa$, on the other hand, is the sum of the photon escape rate Γ due to the cavity opening, and the absorption rate κ accounting for all other loss mechanisms of the radiation inside the resonator. While here κ may be considered fixed, the photon escape rate depends on the resonator mode u . Thus, inasmuch as the resonator mode represents wave chaos, Γ , and therefore C , become random numbers. The distribution $P(\Gamma)$ over an ensemble of modes in time-reversal invariant cavities is a well-know result from random-matrix theory [148,149], and is given by the χ_ν^2 distribution. Here, ν is an integer, counting the number of escape channels at the opening of the resonator. For the case $\nu = 1$, the corresponding distribution is known as the Porter–Thomas distribution.

For a single-mode laser, the mean output intensity is given by $I = \Gamma \langle n \rangle$, where $\langle n \rangle$ is the mean photon number inside the cavity. Over an ensemble of chaotic cavity modes the mean output intensity fluctuates from one mode to the other. Its distribution is given by

$$P(I) = \int d\Gamma P(\Gamma) \delta(I - \Gamma \langle n \rangle). \quad (16)$$

Note that the right-hand side involves a twofold average, the quantum optical average with the distribution P_n (represented by the brackets $\langle \dots \rangle$) and the ensemble average over the cavity modes with distribution $P(\Gamma)$. We evaluate numerically $P(I)$. The results for an ensemble of chaotic cavities with one escape channel are plotted in Fig. 14, for two different sets of parameters. In both cases $A > \bar{C}$, i.e., they correspond to lasers above threshold in the ensemble average. We note that all distributions are strongly non-Gaussian. They are all peaked as $I^{-1/2}$ at small intensities, and present a second peak for maximal intensity. Furthermore, for one of the parameter sets (dashed lines) the distribution $P(I)$ displays a shoulder for submaximal I . This last feature is seen to be a signature of spontaneous emission [142]. Thus, for lasers in resonators with irregular shape the chaotic nature of the cavity modes gives rise to fluctuations of the photocount *on top* of the quantum optical fluctuations known from laser theory. Chaos-induced fluctuations are found when a single-mode photodetection is performed over an ensemble of modes.

In recent years, in the light of nonlinear optical effects, the investigation on multiple scattering of photons has received new impetus. A fresh and fertile field for

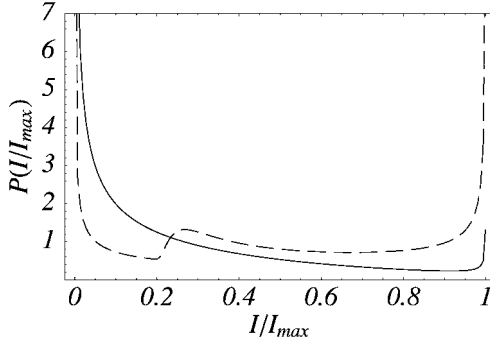


FIG. 14. Distribution $P(I/I_{\max})$ as a function of the dimensionless mean intensity I/I_{\max} , for one escape channel and two sets of parameters. Rates are given in units of $A \equiv 1$, the nonlinearity is $B = 0.005$. The solid line corresponds to $\kappa = 0.7$, $\bar{\Gamma} = 0.02$; the dashed line to $\kappa = 0.7$, $\bar{\Gamma} = 0.2$.

interesting physics is found in this region where nonlinear optics and wave chaos intersect. Random lasers are just one example of the kind of problems encountered there. Other relevant examples constitute studies of coherent backscattering of light by a cloud of cold atoms. In these system, for sufficiently high intensities of the incident light, nonlinearities becomes relevant and a new class of coherent effects are seen to arise [150,151]. In the near future, new questions concerning the consequences of nonlinear effects for the strong localization of light are likely to move into focus.

3.5. DIRECTED ATOMIC TRANSPORT DUE TO INTERACTION-INDUCED QUANTUM CHAOS

All the above examples of transport in quantum chaotic systems stem from the realm of one (active) particle dynamics—where we also include the phenomena observed with alkaline atoms, since the multielectron atomic core only induces additional quantum diffraction effects, which can be accounted for on the one particle level. In our last example, we consider now an interacting many-particle problem, which is motivated by recent progress in the manipulation of ultracold atoms loaded into optical lattices, and which establishes, in some sense, the experimentally “controlled” version of multiparticle quantum chaos originally thought of by Bohr [152] and Wigner [153] when they modelled compound nuclear reactions.

One of the prominent models to describe the dynamics of matter waves in optical potentials is defined by the Bose–Hubbard Hamiltonian (2) which we already encountered above. Indeed, it can be shown that (2) exhibits Wigner–Dyson statistics in a broad interval of tunneling coupling J and interaction strength W , for

filling factors $\bar{n} = N/L$, N the particle number and L the lattice length, even in the absence of any static forcing, i.e., for $F = 0$ [154]. Surprisingly, this was realized only recently, despite the fact that (2) is a standard “working horse” for quite a big community—which, however, is mostly interested in ground state properties rather than dynamics. Only recent experiments in quantum optics laboratories [8, 155–160] have triggered enhanced interest in dynamics, and hence in the excitation spectrum of the many-body Hamiltonian.

On the dynamical level, the chaotic character of the Bose–Hubbard spectrum induces the rapid decay of single particle Bloch oscillations across a one-dimensional lattice, for not too large static forcing (such that the static term in (2) does not dominate the symmetry of the problem) [161,162]. The single particle dynamics can be defined equally well by the reduced single particle wave function of the bosonic ensemble, or by a second, spin-polarized fermionic component loaded into the lattice [163]. We shall here adopt the latter scenario, where non-interacting fermionic atoms interact with a bosonic “bath”. The corresponding two-component Hamiltonian writes

$$H_{\text{FB}} = H_{\text{F}} + H_{\text{B}} + H_{\text{int}}, \quad (17)$$

and decomposes into the (single particle) fermionic part

$$H_{\text{F}} = -\frac{J_{\text{F}}}{2} \left(\sum_{l=1}^L |l+1\rangle\langle l| + \text{h.c.} \right) + Fd \sum_{l=1}^L |l\rangle\langle l|, \quad (18)$$

the (many particle) bosonic part

$$H_{\text{B}} = -\frac{J_{\text{B}}}{2} \left(\sum_{l=1}^L \hat{a}_{l+1}^\dagger \hat{a}_l + \text{h.c.} \right) + \frac{W_{\text{B}}}{2} \sum_{l=1}^L \hat{n}_l (\hat{n}_l - 1), \quad (19)$$

and a term which mediates the collisional interaction between fermions and bosons,

$$H_{\text{int}} = W_{\text{FB}} \sum_{l=1}^L \hat{n}_l |l\rangle\langle l|. \quad (20)$$

Here we built in the assumption that only the fermions experience the external static force—this can be arranged by preparing the fermionic and bosonic component in appropriate internal electronic states, which couple differently to external fields.

Since in (17) there is a clear separation between “system” (the fermions) and “bath” (the bosons), we can derive a master equation for the time evolution in the fermionic degree of freedom, in Markovian approximation [163]. A crucial ingredient for this derivation is the chaotic level dynamics of the bath degree of freedom, what ensures a broad distribution of frequencies of the bath modes, such

as to act as a Markovian environment, with a rapid decay of the bath correlations, on the relevant time scales of the system dynamics [164]. One ends up with

$$\frac{\partial \rho_{l,m}^{(F)}}{\partial t} = -\frac{i}{\hbar} [H_F(t), \rho^{(F)}]_{l,m} - \gamma(1 - \delta_{l,m})\rho_{l,m}^{(F)}, \quad (21)$$

where ρ is the fermionic one particle density matrix, and the relaxation rate γ is completely determined by the parameters of our original Hamiltonian (17):

$$\gamma = \frac{\tau \bar{n}^2 W_{\text{FB}}^2}{\hbar^2} \simeq \frac{3\bar{n}^2 W_{\text{FB}}^2}{\hbar J_B}. \quad (22)$$

In other words, we can “engineer” incoherent Markovian dynamics in a perfectly Hamiltonian system, (17), by exploiting the chaotic dynamics of one system component. The resulting decay of the fermionic Bloch oscillations is illustrated in Fig. 15, where perfect agreement of the actual decay rate (resulting from an exact numerical propagation of the dynamics generated by (17)) with the analytical expression (22) is observed.

The collisional interaction of the fermions with the bosonic bath provides a relaxation mechanism which, in the theory of electronic conductance across a periodic potential, is the necessary ingredient for observing a net current across the lattice [165]. Yet, in Fig. 15 we do not observe any net drift of the electrons. This

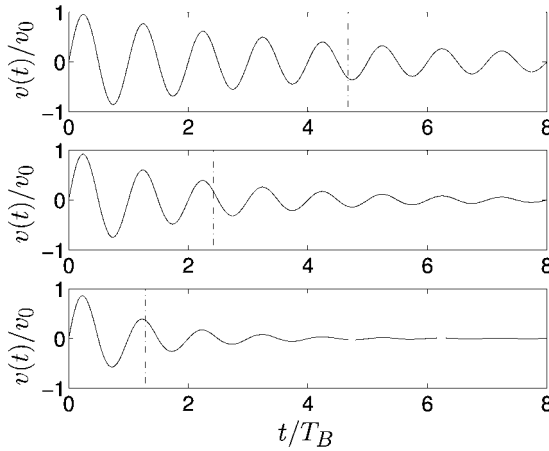


FIG. 15. Bloch oscillations of the fermionic mean velocity in the optical lattice, under a static tilt $Fd = 0.57 \times J_F$, with $J_F = J_B$, and $W_{\text{FB}} = 0.101 \times J_F, 0.143 \times J_F, 0.202 \times J_F$ (from top to bottom). The bosonic bath, which is the source of the collisionally induced damping of the oscillations, is composed of $N = 7$ particles, distributed over a lattice of length $L = 9$. $v_0 = J_F d / \hbar$. The typical time scale of the interaction induced decay fits the time scale predicted by Eq. (22) (dash-dotted lines) very well [163].

is due to the fact that we are here dealing with a perfectly closed system, without attaching any leads—in particular, we are dealing with a *finite size* bath, which, consequently, has a finite heat capacity. Therefore, the initial state of the bath plays a crucial role for the effective fermionic transport across the optical lattice: If prepared in the thermalized state (as in Fig. 15), with equal population of all energy levels of the bath, no net energy flux can occur from the fermionic into the bosonic degree of freedom, and, hence, no net drift velocity of the fermions can emerge. In contrast, if we prepare the bath in a low temperature state, with only the ground state and few excited states initially populated, the bath can absorb energy from the fermions, via collisions, and the fermionic component acquires a non-vanishing drift—which lasts until the bath is fully thermalized. This is illustrated in Fig. 16, together with the corresponding energy increase of the bath. Figure 17 shows the resulting current (fermionic drift velocity \bar{v}) voltage (static tilt F experienced by the fermionic component) characteristics under variations of F , which displays a marked transition from Ohmic behavior (small F) to negative differential conductance (large F)! Note that such behavior was earlier predicted for semiconductor superlattices [166], on the basis of a semiclassical theory with a phenomenologically determined relaxation rate γ , whereas the present scenario allows for the experimental tuning of the relaxation rate, on the basis of our microscopic theory (with crucial input from the theory of quantum chaos).

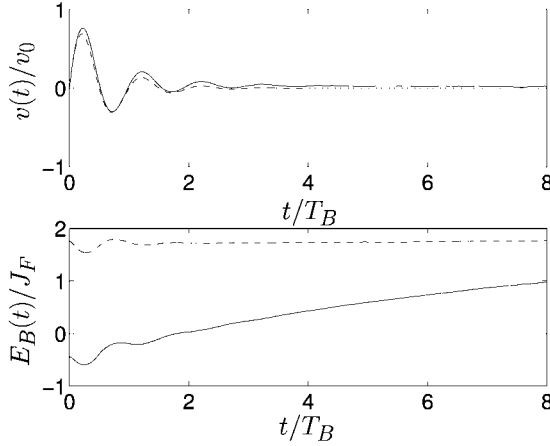


FIG. 16. Mean velocity $v(t)$ of the fermionic component (top, solid line) for a low temperature ($k_B T \simeq 2.86 \times J_B$) bath, under static tilt $Fd = 0.143 \times J_F$, with $W_{FB} = 0.143 \times J_F$, $W_B/J_B = 3/7$, $J_B = J_F$, $N = 7$, $L = 9$. The solid line in the bottom plot shows the associated time evolution of the mean energy E_B of the bath. Dashed lines in both plots indicate the result for a thermalized bath ($k_B T \simeq 150 \times J_B$), when no net energy exchange between the fermions and the bosons is possible. Clearly, only for the low temperature bath do we observe a nonvanishing drift velocity (i.e., a directed current) of the fermions across the lattice.

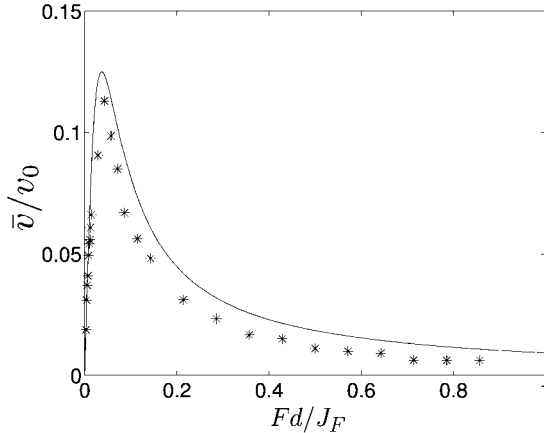


FIG. 17. Current–voltage (expressed as drift velocity \bar{v} vs. tilt Fd) characteristics for the directed fermionic current across the optical lattice (stars) [163], for the same parameters as in Fig. 16. The continuous line shows the prediction of a phenomenological model of charge transport in semiconductor superlattices [166], with the relaxation rate γ extracted from Eq. (22). A clear transition from Ohmic to negative differential conductance at large tilt potentials is observed.

4. Control through Chaos

We have seen in the preceding sections that quantum chaos is tantamount to strong coupling of the various degrees of freedom of a given quantum system, of the destruction of good quantum numbers, and that all this usually leads to large fluctuations of various observables under slight changes of some control parameter, or to decoherence-like reduced dynamics. Though, does quantum chaos provide us with any means not only to describe, but also to control complex quantum systems in a robust way?

Indeed, there is a positive response to this question, at least for periodically driven quantum systems with a mixed regular-chaotic structure of the underlying classical dynamics. The phase space of such systems decomposes into domains of regular and of chaotic motion, see Fig. 18, which are associated with elliptic (i.e., stable) and hyperbolic (i.e., unstable) periodic orbits. Elliptic periodic orbits are surrounded by elliptic islands in phase space, which define regions of regular, i.e., integrable classical motion. A classical particle launched within such an island cannot leave it (or, in higher dimensions, only on rather long time scales [167,168]), and the only way for a quantum particle to leave the island is by tunneling. It is rather obvious on semiclassical grounds [169], and has also been realized by approximating the quantum dynamics in elliptic islands by a quantum pendulum [170], that such regular regions in classical phase space lend support for quantum eigenstates localized on top of them, provided the island’s volume

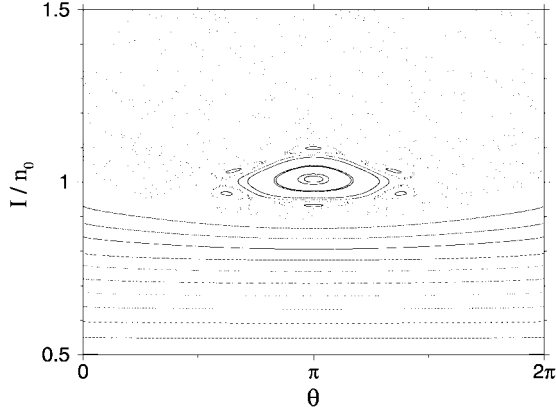


FIG. 18. Example for the surface of section of the classically mixed regular-chaotic phase space of a periodically driven system in a one-dimensional configuration space—here derived from the equations of motion of a one-dimensional hydrogen atom under periodic electromagnetic driving (in dipole coupling) [31]. The phase space—spanned by the classical action I (measured in units of some reference action n_0) and the conjugate angle θ —decomposes into essentially three main components: a near-integrable (weakly perturbed) part (for actions below approx. 0.9), a prominent resonance island structure centered around $(\theta = \pi, I/n_0 = 1.0)$, and a chaotic region—the complement of near-integrable and island domain.

is large enough to accommodate the typical phase space volume \hbar^f (with f the number of degrees of freedom) of a quantum state. Later on it was realized that, in periodically driven systems, these quantum eigenstates faithfully follow the time evolution of the elliptic trajectory they are anchored to [20,171–173], and that their localization properties are preserved by the elliptic island—i.e., by the underlying nonlinearity of the classical dynamics—thus protecting them against the usual dispersion of quantum wave packets in unharmonic systems. Hence, elliptic islands in classical phase space give rise to the emergence of *nondispersive* wave packets on the quantum level [31]. The only mechanism which limits their life time (as long as incoherent processes can be excluded [31,174,175]) is tunneling from the island into the surrounding chaotic sea, which, however, is strongly suppressed in the semiclassical limit of large classical actions as compared to \hbar [176].

Since elliptic structures in mixed regular chaotic classical dynamics are ubiquitous, so are nondispersive wave packets in the microscopic world. And the classical nonlinear dynamics bears yet another blessing: The KAM theorem guarantees that elliptic islands in classical phase space are extremely robust against perturbations—i.e., for sufficiently small perturbations, an elliptic island is possibly slightly distorted in phase space, though preserves its topology. While KAM might appear of essentially mathematical interest on a first glance, this statement has indeed very far-reaching consequences on the experimental level: Note that it

is very hard to prevent conventional Rydberg wave packets, built, e.g., on a Stark manifold (by exciting a coherent superposition of the Stark levels, with a laser pulse, from the atomic ground state) from dispersion [71]—since any small (uncontrolled) perturbation shifts the Stark levels and thus induces an unharmonicity in the spectrum, leading to dispersion of the wave packet. In contrast, a nondispersive wave packet anchored to an elliptic island in classical phase space is essentially inert against any perturbation which is not strong enough to destroy the island, as a consequence of KAM. In other words, the KAM theorem as one of the fundamental theorems of classical nonlinear dynamics shields nondispersive wave packets against technical noise (alike stray fields, etc.). It is this robustness which allows the experimentalist to realize and manipulate nondispersive wave packets in the laboratory [28], over time scales which exceed “traditional” wave packet dynamics by orders of magnitude!

4.1. NONDISPERSIVE WAVE PACKETS IN ONE PARTICLE DYNAMICS

The simplest realization of nondispersive wave packets is provided by an unharmonic, bounded, one-dimensional system under periodic driving, described by the Hamiltonian

$$H_{\text{wp}} = H_0(z) + \lambda V(z) \cos(\omega t). \quad (23)$$

Transformation to the action-angle variables (I, θ) of H_0 allows one to rewrite this as

$$H_{\text{wp}} = H_0(I) + \lambda \sum_{m=-\infty}^{m=+\infty} V_m(I) \cos(m\theta - \omega t), \quad (24)$$

where we assumed, for simplicity, that the Fourier amplitudes $V_m(I)$ are real [31]. Reminding ourselves of $\theta = \Omega t$, with Ω the classical roundtrip frequency along the unperturbed trajectory with action I , we immediately realize that choices of the driving frequency ω such that $s\theta - \omega t \simeq 0$, for some term $m = s$ in the above sum in (24), will lead to a separation of time scales in the time evolution generated by H_{wp} . While all terms in (24) except the one with $m = s$ will oscillate rapidly, a resonance will occur between the external drive at frequency ω and the unperturbed motion along the trajectory with $s\Omega(I) = \omega$. In other words, proper choice of the driving frequency allows one to *selectively* address a specific trajectory of the unperturbed dynamics, via this resonance condition. For $s = 1$, a suitable coordinate transformation, followed by a secular approximation (which averages over the rapidly oscillating terms in (24), at resonance), and a final quadratic expansion around the action of the resonantly driven classical orbit yields a pendulum Hamiltonian, which establishes the backbone of the typical phase space structure of an elliptic island at weak perturbation amplitudes,

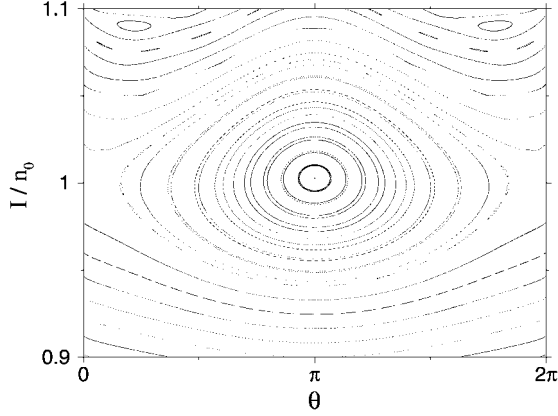


FIG. 19. Typical phase space structure in the vicinity of a resonantly driven trajectory of a bounded, one-dimensional system, in action-angle coordinates I and θ . I is measured in units of some reference action n_0 . The external driving frequency is chosen such as to match the unperturbed roundtrip frequency of the trajectory with action $I/n_0 = 1.0$. The consequent separation of time scales in (24) induces an onion-like, elliptic island structure centered around $(\theta = \pi, I/n_0 = 1.0)$, already at weak perturbation strengths λ . With increasing λ chaos invades phase space, at the expense of the elliptic island and of near integrable regions at low actions. However, comparison with Fig. 18 also shows that the center of the elliptic island survives (actually to rather large values of λ [31,63]), what is a consequence of the KAM theorem, and identifies elliptic islands as very robust topological structures in classical phase space.

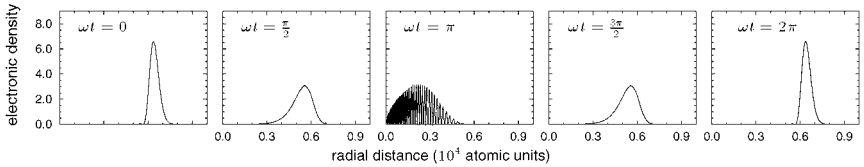


FIG. 20. Electronic density of a nondispersive electronic wave packet in a periodically driven, one-dimensional Rydberg atom. The wave packet starts (at phase $\omega t = 0$ of the driving field) at the outer turning point of the classical eccentricity one orbit, is reflected from the Coulomb singularity at $\omega t = \pi$, and precisely refocuses at the outer turning point, without dispersion, after one complete field cycle.

displayed in Fig. 19. The KAM theorem essentially guarantees that the core of this structure survives even a considerable increase of λ , whilst all the remaining phase space volume may undergo a dramatic metamorphosis, as evident from a comparison of Figs. 18 and 19.

Figure 20 shows the configuration space representation of a nondispersive wave packet launched along the Rydberg orbit with principal quantum number $n_0 = 60$, for the one-dimensional Coulomb problem [20]. This model describes the dynam-

ics of quasi one-dimensional (i.e., extremal parabolic) Rydberg states of atomic hydrogen in a near resonant field reasonably well [96,97]. Such a nondispersive electronic wave packet propagating without dispersion along a highly excited Rydberg orbit has recently been excited and probed in laboratory experiments with lithium atoms [28,29]. In particular, these experiments succeeded to demonstrate the extremely long life time of these objects, by probing the electron's position on its Rydberg orbit after 15,000 cycles of the driving microwave field. This is equivalent to 15,000 Kepler orbits of the unperturbed Coulomb dynamics, and thus by approximately three orders of magnitude longer than the life time of any Rydberg wave packet so far generated in the laboratory. Furthermore, the experimentally measured life time only gives a lower bound for the wave packet's endurance, since longer probing times were not possible due to the geometry of the experimental setup. Theory predicts life times of approx. 10^6 Kepler orbits, at these excitations [31,176].

4.2. NONDISPERSIVE WAVE PACKETS IN THE THREE BODY COULOMB PROBLEM

The above scenario of nondispersive one particle wave packets can be generalized for the three body Coulomb problem, naturally realized in the helium atom. A very nontrivial complication arises here from the fact that the electron–electron interaction term in the helium Hamiltonian

$$H_{\text{He}} = \frac{\mathbf{p}_1^2}{2} + \frac{\mathbf{p}_2^2}{2} - \frac{2}{r_1} - \frac{2}{r_2} + \frac{1}{|\mathbf{r}_1 - \mathbf{r}_2|}, \quad (25)$$

generates classically chaotic dynamics even in the absence of any external perturbation [39]. This is nowadays identified as the cause of the failure of the early semiclassical quantum theory to come up with a quantitative description of the helium spectrum [41]. Furthermore, doubly excited states of helium have a finite autoionization probability, again due to the electron–electron interaction [177,178]. Hence, the helium atom itself has to be treated as an open system, and bears some similarity with the crossed fields problem which we discussed in Section 3.3 above. Indeed, Ericson fluctuations are also expected in the photoabsorption cross section of helium [179], for sufficiently high excitations, though the required energy range has not yet been reached in the lab [23].

Thus, since the classical phase space structure of the helium atom is globally chaotic, our above motivation of the typical elliptic island structure on which to build nondispersive wave packets is not straightforward, since there are no global action-angle variables for irregular classical dynamics. However, we can focus on specific regular domains in the classical phase space of the helium

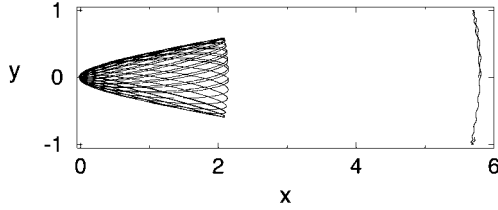


FIG. 21. Characteristic frozen planet trajectory of the unperturbed three body Coulomb problem. The inner electron precesses on highly eccentric ellipses, with a rapid Kepler oscillation between the inner and the outer turning point. Upon average over the inner electron’s rapid motion, Coulomb attraction due to the screened Coulomb potential of the nucleus and electron–electron repulsion conspire such as to create an adiabatic, shallow binding potential for the outer electron [181]. Consequently, the outer electron is locked upon the precessing motion of the inner electron, leading to a strong correlation of both electrons’ positions.

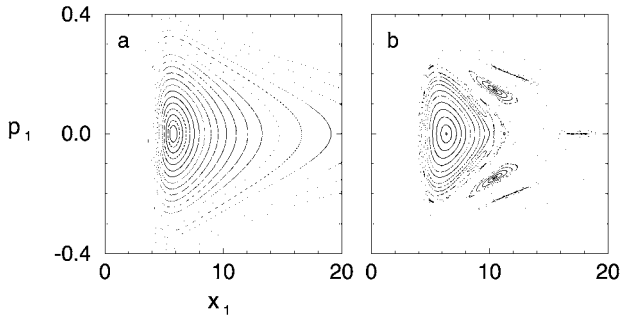


FIG. 22. Phase space structure for the outer electron of the (collinear) frozen planet configuration [182], in the absence (a) and in the presence (b) of an external, near resonant driving field. If the external field frequency is chosen to match a resonance condition with the unperturbed outer electron’s motion, secondary resonance islands emerge as in (b).

atom, which are elliptic islands themselves.² These lend support for stable eigenstates of the unperturbed helium atom—the most prominent thereof being the frozen planet configuration [36,180]. Figures 21 and 22 show a typical classical, highly correlated two-electron trajectory, and the phase space structure of the frozen planet configuration, respectively. Given the regular phase space structure with well-defined, stable periodic orbits as shown in Fig. 22, we are back to our original setting: If we apply an external field with a frequency near

² Indeed, by mapping an f degrees of freedom system on a periodically driven $f - 1$ degrees of freedom system, where the periodic time dependence of the drive is provided by the periodic time dependence of the remaining degree of freedom, these islands can be made formally equivalent to those considered above [31,47].

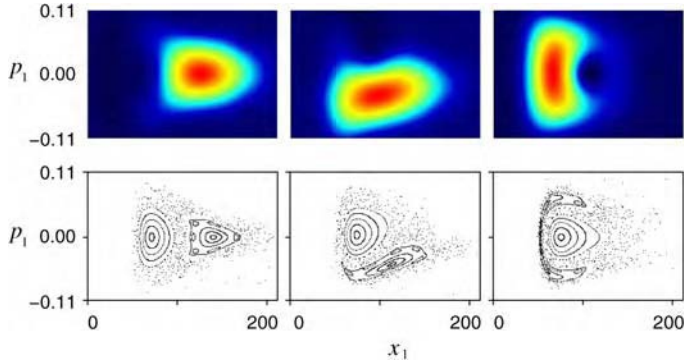


FIG. 23. Top: Husimi representation of a nondispersive two-electron wave packet propagating along the collinear frozen planet orbit of the planar helium atom [184], in the phase space coordinates of the outer electron along the quantization axis defined by the linear field polarization vector, for different phases $\omega t = 0$ (left), $\pi/2$ (middle), and π (right). Very clearly, the electronic density faithfully traces the resonantly driven frozen planet trajectory, as obvious from a comparison with the classical phase space structure shown below (on identical scales).

resonant with one of the stable periodic orbits of the classical phase space of the unperturbed system, we induce elliptic islands which propagate along the unperturbed trajectory, phase-locked on the period of the drive. Consequently, for sufficiently high excitations, we find nondispersive two-electron wave packets [182,183] propagating along the frozen planet trajectory, as illustrated in Fig. 23 for an excitation to the fifth autoionization channel (in other words, the inner electron is launched along an extremal parabolic orbit with principal quantum number $N = 6$). Note that a quantum treatment of the planar three body Coulomb problem (an accurate treatment of the fully three-dimensional problem is hitherto out of reach, due to the size of Hilbert space when many angular momenta are coupled by the driving field) predicts life times of approx. 1000 driving field periods (or, due to the resonance condition on drive and unperturbed two-electron orbit, 1000 frozen planet periods) for these wave packet eigenstates [184,185]. This prediction can be expected to be reliable, on the basis of a comparison of typical He autoionization rates in 1D, 2D, and 3D configuration space [186]. The predicted two-electron wave packet's life times are considerably less than the life times predicted for the one electron problem considered in the previous section, though still much longer than life times of conventional Rydberg wave packets, and thus eligible for applications in coherent control. Recently, the excitation of another type of nondispersive two-electron wave packets has been suggested, with both electrons far from the nucleus [187].

4.3. QUANTUM RESONANCES IN THE DYNAMICS OF KICKED COLD ATOMS

Nondispersive wave packets as those discussed above are ubiquitous, and can be realized in any driven quantum system with an unharmonic spectrum (the unharmonicity guarantees the selectivity of the addressing of a specific classical trajectory by the near resonant drive) and mixed regular-chaotic phase space [31].

Importantly though, their creation is not necessarily restricted to the realm of semiclassical physics, where \hbar becomes small in comparison to the classical actions of the dynamics. This has been realized recently, in the treatment of quantum resonances [188] and quantum accelerator modes [189] in the translational degree of freedom of periodically kicked cold atoms loaded into one-dimensional optical lattices which are flashed periodically. Such quantum resonances occur due to the close similarity of the kicked atom Hamiltonian

$$H_{\text{KA}} = \frac{p^2}{2} - K \cos(kx) \sum_{m=-\infty}^{+\infty} \delta(t - m\tau) \quad (26)$$

with the kicked rotor, apart from the different boundary conditions (an infinite periodic lattice in the atomic problem, a circle in the case of the kicked rotor [188]). They are excited by kicking periods $\tau = 2\pi\ell$, ℓ integer, since then the kicks are synchronized with the exact revivals of the free evolution of the rotor dynamics (we omit here the discussion of the specific value of the atomic quasimomentum, which implies further restrictions, though is not indispensable for our present argument), leading to ballistic energy growth, for the appropriately prepared initial quasimomentum state of the atoms [188].

If one considers the quantum dynamics *close* to the resonance condition, i.e., at $\tau = 2\pi\ell + \epsilon$, with a small detuning ϵ , it turns out [188,189] that the time evolution generated by the Hamiltonian (26) can be obtained from the formal quantization of some well-defined classical dynamics described by a map, with the detuning ϵ taking the role of $\hbar \equiv \tau$ (which itself remains constant and can be arbitrarily large!).

The quantum accelerator modes are created when an additional static potential (such as provided by gravity) is added to the Hamiltonian of Eq. (26). For appropriate parameters, this Stark field allows the experimentalist to design classical nonlinear-resonance islands (classical in the above sense of ϵ taking the role of \hbar) embedded in a surrounding chaotic sea. These islands support ballistic transport, which—in contrast to the ballistic motion at quantum resonance—is directed due to the destruction of the translational invariance by the Stark field (see the accelerated tail of the atoms' momentum distribution in Fig. 24).

In this generalized classical picture, both quantum resonances and quantum accelerator modes are nothing but quantum eigenstates anchored to elliptic islands in the phase space of that classical map, i.e., a variant of our above nondispersive

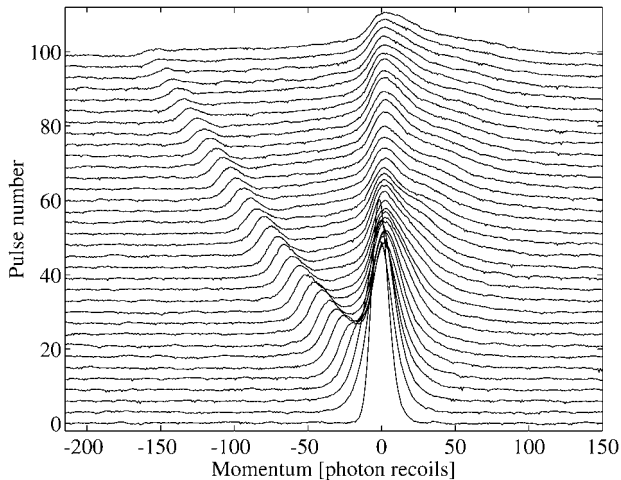


FIG. 24. (Courtesy of Gil Summy.) Time dependence (measured by the number of pulses or kicks) of the atomic momentum distribution under periodic kicks along the gravitational field [15], in a reference frame freely falling with the atoms. Besides the bulk of the atomic ensemble, which does not acquire momentum, there is an atomic component which exhibits ballistic acceleration. This is the experimental signature of a quantum accelerator mode.

wave packets. This mode-locking of the external drive to the intrinsic characteristic frequency of the system allows the experimentalist to efficiently transfer large momenta to the atoms. Once again, these modes are robust against perturbations [190], are clearly identifiable in laboratory experiments [14–16], see Fig. 24, and offer a variety of experimental applications, such as for high precision measurements of the gravitational constant [14].

5. Conclusion

As quantum optics addresses the dynamics of more and more complex quantum systems, methods imported from quantum chaos provide useful tools for identifying statistically robust quantities for their description, and also to control their time evolution. In this review, we have seen examples for characteristic universal features of chaotic quantum systems on the spectral as well as on the dynamical level, in such different settings like ultracold atoms in periodic optical potentials, excitation and ionization processes of one and two-electron atoms subject to static or oscillating external fields, random laser theory, and cold atoms kicked by standing light fields. The chosen examples are far from exploring all the diversity of current experimental and theoretical activities at the interface of quantum

optics and chaos—we did not discuss here the recently predicted and observed universal ionization threshold of one electron Rydberg states under microwave driving [84,117], weak and strong localization phenomena in the scattering of photons off clouds of cold (or ultracold) trapped atoms (with close connections to random lasing) [191], nor the complementary scenario of matter wave transport in disordered optical or magnetic potentials [10,115], or the role of incoherent processes which might compete with coherent quantum transport in complex dynamics [12,86,174,175]. Nonetheless, we hope that the examples treated already give a flavor of the potential applications of quantum chaos, from the microscopic modelling of an atomic current across a periodic potential, by using a chaotic bosonic system as a bath which provides the necessary relaxation processes, to nondispersive, one and two-electron wave packets which, due to their extraordinarily long life times and robustness against technical noise (inherited from the KAM theorem), might find applications in robust quantum control schemes or as quantum memory, in the context of quantum information processing. In particular, the analogies between quantum chaos and quantum transport in disordered systems are currently coming into focus, and hold a panoply of intriguing challenging questions, to be tackled in the near future.

6. References

- [1] F. Haake, “Quantum Signatures of Chaos”, *Springer Series in Synergetics*, vol. 54, Springer, Berlin, 1991.
- [2] W. Nagourney, J. Sandberg, H. Dehmelt, *Phys. Rev. Lett.* **56** (1986) 2797.
- [3] T. Sauter, W. Neuhauser, R. Blatt, P. Toschek, *Phys. Rev. Lett.* **57** (1986) 1696.
- [4] D. Meschede, H. Walther, G. Müller, *Phys. Rev. Lett.* **54** (1985) 551.
- [5] M. Brune, E. Hagley, J. Dreyer, X. Maître, A. Maali, C. Wunderlich, J.-M. Raimond, S. Haroche, *Phys. Rev. Lett.* **77** (1996) 004887.
- [6] T. Jennewein, C. Simon, G. Weihs, H. Weinfurter, A. Zeilinger, *Phys. Rev. Lett.* **87** (2000) 4729.
- [7] W. Hensinger, H. Häffner, A. Browaeys, N. Heckenberg, K. Helmerson, C. McKenzie, G. Milburn, W. Phillips, S. Rolston, H. Rubinsztein-Dunlop, et al., *Nature* **412** (2000) 52.
- [8] M. Greiner, O. Mandel, T. Esslinger, T.W. Hänsch, I. Bloch, *Nature* **415** (2002) 39.
- [9] T.P. Meyrath, F. Schreck, J.L. Hanssen, C.-S. Chu, M.G. Raizen, *Phys. Rev. A* **71** (2005) 41604.
- [10] J. Lye, L. Fallani, M. Modugno, D. Wiersma, C. Fort, M. Inguscio, *Phys. Rev. Lett.* **95** (2005) 070401.
- [11] A. Buchleitner, R.N. Mantegna, *Phys. Rev. Lett.* **80** (1998) 3932.
- [12] T. Wellens, S. Shatkhin, A. Buchleitner, *Rep. Prog. Phys.* **67** (2004) 45.
- [13] J.C. Robinson, C. Bharucha, F.L. Moore, R. Jahnke, G.A. Georgakis, Q. Niu, M.G. Raizen, B. Sundaram, *Phys. Rev. Lett.* **74** (1995) 3963.
- [14] A. Buchleitner, M. d’Arcy, S. Fishman, S. Gardiner, I. Guarneri, Z.-Y. Ma, L. Rebuzzini, G. Summy, physics/0501146, 2005.
- [15] M. Oberthaler, R. Godun, M. d’Arcy, G. Summy, K. Burnett, *Phys. Rev. Lett.* **83** (1999) 4447.
- [16] S. Schlunk, M. d’Arcy, S. Gardiner, G. Summy, *Phys. Rev. Lett.* **90** (2003) 124102.
- [17] F.L. Moore, J.C. Robinson, C. Bharucha, P.E. Williams, M.G. Raizen, *Phys. Rev. Lett.* **73** (1994) 2974.

- [18] M.B. d’Arcy, R. Godun, G.S. Summy, I. Guarneri, S. Fishman, S. Wimberger, A. Buchleitner, *Phys. Rev. E* **69** (2004) 027201.
- [19] J. Ringot, P. Szriftgiser, J.C. Garreau, D. Delande, *Phys. Rev. Lett.* **85** (2000) 2741.
- [20] D. Delande, A. Buchleitner, *Adv. At. Mol. Opt. Phys.* **35** (1994) 85.
- [21] A. Buchleitner, D. Delande, J. Zakrzewski, R.N. Mantegna, M. Arndt, H. Walther, *Phys. Rev. Lett.* **75** (1995) 3818.
- [22] C. Iu, G.R. Welch, M.M. Kash, D. Kleppner, D. Delande, J.C. Gay, *Phys. Rev. Lett.* **66** (1991) 145.
- [23] R. Püttner, B. Grémaud, D. Delande, M. Domke, M. Martins, A. Schlachter, G. Kaindl, *Phys. Rev. Lett.* **86** (2001) 3747.
- [24] P. Szriftgiser, J. Ringot, D. Delande, J.C. Garreau, *Phys. Rev. Lett.* **89** (2002) 224101.
- [25] M. Geisler, J. Smet, V. Umansky, K. von Klitzing, B. Naundorf, R. Ketzmerick, H. Schweizer, *Phys. Rev. Lett.* **92** (2004) 256801.
- [26] A. Sachrajda, R. Ketzmerick, C. Gould, Y. Feng, P. Kelly, A. Delage, Z. Wasilewski, *Phys. Rev. Lett.* **80** (1998) 001948.
- [27] G. Stania, H. Walther, *Phys. Rev. Lett.* **95** (2005) 194101.
- [28] H. Maeda, T. Gallagher, *Phys. Rev. Lett.* **92** (2004) 133004.
- [29] H. Maeda, D. Norum, T.F. Gallagher, *Science* **307** (2005) 1757.
- [30] S. Wimberger, M. Sadgrove, S. Parkins, R. Leonhardt, *Phys. Rev. A* **71** (2005) 053404.
- [31] A. Buchleitner, D. Delande, J. Zakrzewski, *Phys. Rep.* **368** (2002) 409.
- [32] A.R.R. de Carvalho, A. Buchleitner, *Phys. Rev. Lett.* **92** (2004) 204101.
- [33] M. Gutzwiller, The semi-classical quantization of chaotic Hamiltonian systems, in: “Chaos and Quantum Physics”, North-Holland, Amsterdam, 1991, p. 201.
- [34] E. Heller, Wavepacket dynamics and quantum chaology, in: “Chaos and Quantum Physics”, North-Holland, Amsterdam, 1991, p. 547.
- [35] U. Smilansky, The classical and quantum theory of chaotic scattering, in: “Chaos and Quantum Physics”, North-Holland, Amsterdam, 1991, p. 371.
- [36] K. Richter, D. Wintgen, *Phys. Rev. Lett.* **65** (1990) 1965.
- [37] D. Wintgen, A. Bürgers, K. Richter, G. Tanner, *Prog. Theor. Phys. Supplement* (1994) 121.
- [38] D. Wintgen, K. Richter, G. Tanner, *CHAOS* **2** (1992) 19.
- [39] K. Richter, G. Tanner, D. Wintgen, *Phys. Rev. A* **48** (1993) 4182.
- [40] G. Tanner, D. Wintgen, *Phys. Rev. Lett.* **75** (1995) 2928.
- [41] G. Tanner, K. Richter, J. Rost, *Rev. Mod. Phys.* **72** (2000) 497.
- [42] D. Delande, Chaos in atomic and molecular physics, in: “Chaos and Quantum Physics”, North-Holland, Amsterdam, 1991, p. 665.
- [43] O. Bohigas, Random matrix theories and chaotic dynamics, in: “Chaos and Quantum Physics”, North-Holland, Amsterdam, 1991, p. 87.
- [44] A.R. Kolovsky, A. Buchleitner, *Phys. Rev. E* **68** (2003) 056213.
- [45] D. Jaksch, C. Bruder, J.I. Cirac, C.W. Gardiner, P. Zoller, *Phys. Rev. Lett.* **81** (1998) 3108.
- [46] M.L. Mehta, “Random Matrices”, Academic Press, San Diego, 1991.
- [47] A.J. Lichtenberg, M.A. Lieberman, “Regular and Stochastic Motion”, in: *Applied Mathematical Sciences*, vol. 38, Springer, Berlin, 1983.
- [48] T. Fromhold, A. Patanè, S. Bujkiewicz, P. Wilkinson, D. Fowler, D. Sherwood, S. Stapleton, A. Krokhin, L. Eaves, M. Henini, et al., *Nature* **428** (2004) 726.
- [49] A. Chernikov, R. Sagdeev, D. Usikov, M. Zakharov, G. Zaslavsky, *Nature* **326** (1987) 559.
- [50] K.A.H. van Leeuwen, G. von Oppen, S. Renwick, J.B. Bowlin, P.M. Koch, R.V. Jensen, O. Rath, D. Richards, J.G. Leopold, *Phys. Rev. Lett.* **55** (1985) 2231.
- [51] T. Geisel, G. Radons, J. Rubner, *Phys. Rev. Lett.* **57** (1986) 2883.
- [52] R.V. Jensen, *Physica Scripta* **35** (1987) 668.
- [53] G. Casati, B.V. Chirikov, D.L. Shepelyansky, I. Guarneri, *Phys. Rep.* **154** (1987) 77.

- [54] G. Radons, R.E. Prange, *Phys. Rev. Lett.* **61** (1988) 1691.
- [55] R. Blümel, C. Hillermeier, U. Smilansky, *Z. Phys. D* **15** (1990) 267.
- [56] R.V. Jensen, S.M. Susskind, M.M. Sanders, *Phys. Rep.* **201** (1991) 1.
- [57] W. Jans, T. Monteiro, W. Schweizer, P. Dando, *J. Phys. A* **26** (1993) 3187.
- [58] J.G. Leopold, D. Richards, *J. Phys. B: Atom. Mol. Opt. Phys.* **27** (1994) 2169.
- [59] K. Dietz, J. Henkel, M. Holthaus, *Phys. Rev. A* **45** (1992) 4960.
- [60] P.M. Koch, K.A.H. van Leeuwen, *Phys. Rep.* **255** (1995) 289.
- [61] M.R.W. Bellermann, P.M. Koch, D. Richards, *Phys. Rev. Lett.* **78** (1997) 3840.
- [62] A. Buchleitner, D. Delande, *Chaos, Solitons and Fractals* **5** (1995) 1125.
- [63] J. Zakrzewski, A. Buchleitner, D. Delande, *Z. Phys.* **B103** (1997) 115.
- [64] A. Krug, Ph.D. thesis, Ludwig-Maximilians-Universität München, 2001, <http://edoc.uni-muenchen.de/archive/00000336/>.
- [65] H. Held, W. Schweizer, *Phys. Rev. Lett.* **84** (2000) 1160.
- [66] P. Lambropoulos, P. Zoller, *Phys. Rev. A* **24** (1981) 379.
- [67] C. Cohen-Tannoudji, J. Dupont-Roc, G. Grynberg, "Atom-Photon Interactions", Wiley, New York, 1992.
- [68] M. Reed, B. Simon, "Analysis of Operators, Methods of Modern Mathematical Physics", Academic Press, San Diego, 1990.
- [69] A. Buchleitner, B. Grémaud, D. Delande, *J. Phys. B: Atom. Mol. Opt. Phys.* **27** (1994) 2663.
- [70] L. Marmet, H. Held, G. Raithel, J.A. Yeazell, H. Walther, *Phys. Rev. Lett.* **72** (1994) 3779.
- [71] C. Raman, T. Weihnacht, P. Bucksbaum, *Phys. Rev. A* **55** (1997) R3995.
- [72] J.A. Yeazell, J.C.R. Stroud, *Phys. Rev. Lett.* **60** (1988) 1494.
- [73] A. Buchleitner, D. Delande, J.C. Gay, *J. Opt. Soc. Am. B* **12** (1995) 505.
- [74] S. Yoshida, C. Reinhold, J. Burgdörfer, *Phys. Rev. Lett.* **84** (2000) 2602.
- [75] C. Reinhold, W. Zhao, J. Lancaster, F. Dunning, E. Persson, D. Arbó, S. Yoshida, J. Burgdörfer, *Phys. Rev. A* **70** (2004) 033402.
- [76] J.E. Bayfield, P.M. Koch, *Phys. Rev. Lett.* **33** (1974) 258.
- [77] J.E. Bayfield, G. Casati, I. Guarneri, D.W. Sokol, *Phys. Rev. Lett.* **63** (1989) 364.
- [78] L. Sirko, A. Haffmans, M.R.W. Bellermann, P.M. Koch, *Europhys. Lett.* **33** (1996) 181.
- [79] M.R.W. Bellermann, P.M. Koch, D. Mariani, D. Richards, *Phys. Rev. Lett.* **76** (1996) 892.
- [80] D. Richards, J.G. Leopold, P.M. Koch, E.J. Galvez, K.A.H. van Leeuwen, L. Moorman, B.E. Sauer, R.V. Jensen, *J. Phys. B: Atom. Mol. Opt. Phys.* **22** (1989) 1307.
- [81] B.E. Sauer, M.R.W. Bellermann, P.M. Koch, *Phys. Rev. Lett.* **68** (1992) 1633.
- [82] P. Fu, T.J. Scholz, J.M. Hetteema, T.F. Gallagher, *Phys. Rev. Lett.* **64** (1990) 511.
- [83] M.W. Noel, W.M. Griffith, T.F. Gallagher, *Phys. Rev. A* **62** (2000) 63401.
- [84] H. Maeda, T.F. Gallagher, *Phys. Rev. Lett.* **93** (2004) 193002.
- [85] O. Benson, A. Buchleitner, G. Raithel, M. Arndt, R.N. Mantegna, H. Walther, *Phys. Rev. A* **51** (1995) 4862.
- [86] M. Arndt, A. Buchleitner, R.N. Mantegna, H. Walther, *Phys. Rev. Lett.* **67** (1991) 2435.
- [87] R. Blümel, R. Graham, L. Sirko, U. Smilansky, H. Walther, K. Yamada, *Phys. Rev. Lett.* **62** (1989) 341.
- [88] R. Blümel, A. Buchleitner, R. Graham, L. Sirko, U. Smilansky, H. Walther, *Phys. Rev. A* **44** (1991) 4521.
- [89] A. Krug, A. Buchleitner, *Phys. Rev. Lett.* **86** (2001) 3538.
- [90] S. Wimberger, A. Krug, A. Buchleitner, *Phys. Rev. Lett.* **89** (2002) 263601.
- [91] P. Anderson, *Phys. Rev.* **109** (1958) 1492.
- [92] S. Washburn, R.A. Webb, *Adv. Phys.* **35** (1986) 375.
- [93] S. Wimberger, A. Buchleitner, *J. Phys. A* **34** (2001) 7181.
- [94] A. Buchleitner, I. Guarneri, J. Zakrzewski, *Europhys. Lett.* **44** (1998) 162.
- [95] G. Casati, I. Guarneri, D.L. Shepelyansky, *Phys. Rev. A* **36** (1987) 3501.

- [96] N.B. Delone, B.P. Krainov, D.L. Shepelyansky, *Sov. Phys. Usp.* **26** (1983) 551.
- [97] A. Buchleitner, D. Delande, *Phys. Rev. A* **55** (1997) R1585.
- [98] J.-L. Pichard, N. Zanon, Y. Imry, A.D. Stone, *J. Phys. France* **51** (1990) 587.
- [99] G. Casati, I. Guarneri, F.M. Izrailev, L. Molinari, K. Życzkowski, *Phys. Rev. Lett.* **72** (1994) 2697.
- [100] A. Krug, S. Wimberger, A. Buchleitner, *Eur. Phys. J. D* **26** (2003) 21.
- [101] D.J. Thouless, *Phys. Rep.* **13** (1974) 93.
- [102] S.A. Gurvitz, *Phys. Rev. Lett.* **85** (2000) 812.
- [103] A. Chabanov, A. Genack, *Phys. Rev. Lett.* **87** (2001) 233903.
- [104] M. Pacilli, P. Sebbah, C. Vanneste, in: B.A. van Tiggelen, S. Skipetrov (Eds.), “Wave Scattering in Complex Media: From Theory to Applications”, in: *NATO Science Series II*, vol. 107, Kluwer Academic, New York, 2003, pp. 229–239.
- [105] R. Blümel, U. Smilansky, *Phys. Rev. Lett.* **52** (1984) 137.
- [106] G. Casati, B.V. Chirikov, D.L. Shepelyansky, *Phys. Rev. Lett.* **53** (1984) 2525.
- [107] R. Blümel, U. Smilansky, *Phys. Rev. Lett.* **58** (1987) 2531.
- [108] R. Graham, *Comm. At. Mol. Phys.* **25** (1991) 219.
- [109] J.G. Leopold, D. Richards, *J. Phys. B: Atom. Mol. Opt. Phys.* **38** (1988) 2660.
- [110] A. Buchleitner, D. Delande, *Phys. Rev. Lett.* **70** (1993) 33.
- [111] M. Holthaus, G.H. Ristow, D.W. Hone, *Phys. Rev. Lett.* **75** (1995) 3914.
- [112] S. Fishman, D.R. Grempel, R.E. Prange, *Phys. Rev. Lett.* **49** (1982) 509.
- [113] T. Dittrich, U. Smilansky, *Nonlinearity* **4** (1991) 59.
- [114] O.A. Starykh, P.R.J. Jacquod, E.E. Narimanov, A.D. Stone, *Phys. Rev. E* **62** (2000) 2078.
- [115] B. Damski, J. Zakrzewski, L. Santos, P. Zoller, M. Lewenstein, *Phys. Rev. Lett.* **91** (2003) 80403.
- [116] A. Krug, A. Buchleitner, *Phys. Rev. A* **66** (2002) 53416.
- [117] A. Krug, A. Buchleitner, *Phys. Rev. A* **72** (2005) 061402(R).
- [118] T. Ericson, *Phys. Rev. Lett.* **5** (1960) 430.
- [119] P. von Brentano, J. Ernst, O. Hausser, T. Mayer-Kuckuk, A. Richter, W. von Witsch, *Phys. Lett.* **9** (1964) 48.
- [120] R. Blümel, U. Smilansky, *Phys. Rev. Lett.* **60** (1988) 477.
- [121] H. Weidenmüller, *Nucl. Phys. A* **518** (1990) 1.
- [122] F. Borgonovi, I. Guarneri, *J. Phys. A* **25** (1992) 3239.
- [123] G. Stania, Ph.D. thesis, Ludwig-Maximilians-Universität München, 2005.
- [124] J. Madroñero, A. Buchleitner, *Phys. Rev. Lett.* **95** (2005) 263601.
- [125] H. Cao, *Progress in Optics* **45** (2003) 317.
- [126] C. Gmachl, F. Capasso, E.E. Narimanov, J.U. Nöckel, A.D. Stone, J. Faist, D.L. Sivco, A.Y. Cho, *Science* **280** (1998) 1556.
- [127] T. Harayama, S. Sunuda, K.S. Ikeda, *Phys. Rev. A* **72** (2005) 013803.
- [128] H. Cao, J.Y. Xu, S.H. Chang, S.T. Ho, *Phys. Rev. E* **61** (2000) 1985.
- [129] H. Haken, “Laser Theory”, second ed., Springer, Berlin, 1984.
- [130] M. Sargent III, M.O. Scully, W.E. Lamb, “Laser Physics”, Addison–Wesley, 1974.
- [131] A. Siegman, “Lasers”, Oxford University Press, 1986.
- [132] G. Hackenbroich, C. Viviescas, F. Haake, *Phys. Rev. Lett.* **89** (2002) 083902.
- [133] C. Viviescas, G. Hackenbroich, *Phys. Rev. A* **67** (2003) 013805.
- [134] C. Viviescas, G. Hackenbroich, *J. Opt. B* **6** (2004) 211.
- [135] C. Viviescas, Ph.D. thesis, Universität Duisburg-Essen, 2004, <http://miless.uni-duisburg-essen.de/servlets/DocumentServlet?id=11649>.
- [136] A.L. Schawlow, C.H. Townes, *Phys. Rev.* **112** (1958) 1940.
- [137] K. Petermann, *IEEE J. Quantum. Electron.* **15** (1979) 566.
- [138] A.E. Siegman, *Phys. Rev. A* **39** (1989) 1253.
- [139] A.E. Siegman, *Phys. Rev. A* **39** (1989) 1264.

- [140] C.W.J. Beenakker, *Phys. Rev. Lett.* **81** (1998) 1829.
- [141] C.W.J. Beenakker, in: J.P. Fouque (Ed.), “Diffuse Waves in Complex Media”, in: *NATO Science Series C*, vol. 531, Kluwer Academic, Dordrecht, 1999, p. 137.
- [142] G. Hackenbroich, C. Viviescas, B. Elattari, F. Haake, *Phys. Rev. Lett.* **86** (2001) 5262.
- [143] M. Patra, *Phys. Rev. A* **65** (2002) 043809.
- [144] L. Florescu, S. John, *Phys. Rev. Lett.* **93** (2004) 013602.
- [145] L. Florescu, S. John, *Phys. Rev. A* **69** (2004) 046603.
- [146] M.V. Berry, *J. Phys. A* **10** (1977) 2083.
- [147] J.D. Urbina, K. Richter, *J. Phys. A: Math. Gen.* **36** (2003) L495.
- [148] Y.V. Fyodorov, H.-J. Sommers, *J. Math. Phys.* **38** (1997) 1918.
- [149] T. Guhr, A. Müller-Groeling, H.A. Weidenmüller, *Phys. Rep.* **299** (1998) 189.
- [150] V. Shatokhin, C.A. Müller, A. Buchleitner, *Phys. Rev. Lett.* **94** (2005) 043603.
- [151] T. Wellens, B. Grémaud, D. Delande, C. Miniatura, *Phys. Rev. E* **75** (2005) 055603(R).
- [152] N. Bohr, *Nature* **137** (1936) 344.
- [153] E. Wigner, “Group Theory and Its Application to the Quantum Mechanics”, Academic Press, New York, 1959.
- [154] A. Kolovsky, A. Buchleitner, *Europhys. Lett.* **68** (2004) 632.
- [155] O. Morsch, J.H. Müller, M. Cristiani, D. Ciampini, E. Arimondo, *Phys. Rev. Lett.* **87** (2001) 140402.
- [156] M. Cristiani, O. Morsch, J.H. Müller, D. Ciampini, E. Arimondo, *Phys. Rev. A* **65** (2002) 63612.
- [157] S. Burger, F.S. Cataliotti, C. Fort, F. Minardi, M. Inguscio, M.L. Chiofalo, M.P. Tosi, *Phys. Rev. Lett.* **86** (2001) 4447.
- [158] C. Fort, F.S. Cataliotti, L. Fallani, F. Ferlaino, P. Maddaloni, M. Inguscio, *Phys. Rev. Lett.* **90** (2003) 140405.
- [159] M. Modugno, E. de Mirandes, F. Ferlaino, H. Ott, G. Roati, M. Inguscio, *Fortschr. Phys.* **52** (2004) 1173.
- [160] H. Ott, E. de Mirandes, F. Ferlaino, G. Roati, G. Modugno, M. Inguscio, *Phys. Rev. Lett.* **92** (2004) 160601.
- [161] A.R. Kolovsky, *Phys. Rev. Lett.* **90** (2003) 213002.
- [162] A. Buchleitner, A.R. Kolovsky, *Phys. Rev. Lett.* **91** (2003) 253002.
- [163] A. Ponomarev, J. Madroñero, A. Kolovsky, A. Buchleitner, *Phys. Rev. Lett.* **96** (2006) 050404.
- [164] A. Kolovsky, *Phys. Rev. E* **50** (1994) 3569.
- [165] P. Anderson, “Concepts in Solids: Lectures on the Theory of Solids”, Addison–Wesley, New York, 1992.
- [166] L. Esaki, R. Tsu, *IBM J. Res. Develop.* **14** (1) (1970) 61.
- [167] H.S. Dumas, J. Laskar, *Phys. Rev. Lett.* **70** (1993) 2975.
- [168] J. von Milscewski, G.H.F. Diercksen, T. Uzer, *Phys. Rev. Lett.* **76** (1996) 2890.
- [169] A.M.O. de Almeida, “Hamiltonian Systems: Chaos and Quantization”, Cambridge University Press, Cambridge, 1988.
- [170] G.P. Berman, G.M. Zaslavsky, *Phys. Lett.* **61A** (1977) 295.
- [171] Holthaus M., *Chaos, Solitons and Fractals* **5** (1995) 1143.
- [172] I. Białynicki-Birula, M. Kalinski, J.H. Eberly, *Phys. Rev. Lett.* **73** (1994) 1777.
- [173] D. Farelly, E. Lee, T. Uzer, *Phys. Rev. Lett.* **75** (1995) 972.
- [174] K. Hornberger, A. Buchleitner, *Europhys. Lett.* **41** (1998) 383.
- [175] D. Delande, J. Zakrzewski, *Phys. Rev. A* **58** (1998) 466.
- [176] A. Buchleitner, D. Delande, *Phys. Rev. Lett.* **75** (1995) 1487.
- [177] D. Wintgen, D. Delande, *J. Phys. B: Atom. Mol. Opt. Phys.* **26** (1993) L399.
- [178] J.-M. Rost, K. Schulz, M. Domke, G. Kaindl, *J. Phys. B: Atom. Mol. Opt. Phys.* **30** (1997) 4663.
- [179] B. Grémaud, D. Delande, *Europhys. Lett.* **40** (1997) 363.
- [180] U. Eichmann, V. Lange, W. Sandner, *Phys. Rev. Lett.* **64** (1990) 274.

- [181] V.N. Ostrovsky, N.V. Prudov, *J. Phys. B: Atom. Mol. Opt. Phys.* **28** (1995) 4435.
- [182] P. Schlagheck, A. Buchleitner, *Eur. Phys. J. D* **22** (2003) 401.
- [183] P. Schlagheck, A. Buchleitner, *Europhys. Lett.* **46** (1999) 24.
- [184] J. Madroñero, A. Buchleitner, in: S. Wagner, W. Hanke, A. Bode, F. Durst (Eds.), “High Performance Computing in Science and Engineering, Munich 2004”, Springer, Berlin, 2004, p. 329.
- [185] J. Madroñero, Ph.D. thesis, Ludwig-Maximilians-Universität München, 2004, <http://edoc.ub.uni-muenchen.de/archive/00002187/>.
- [186] J. Madroñero, P. Schlagheck, L. Hilico, B. Grémaud, D. Delande, A. Buchleitner, *Europhys. Lett.* **70** (2005) 183.
- [187] M. Kalinski, L. Hansen, D. Farelly, *Phys. Rev. Lett.* **95** (2005) 103001.
- [188] S. Wimberger, I. Guarneri, S. Fishman, *Nonlinearity* **16** (2003) 1381.
- [189] S. Fishman, I. Guarneri, L. Rebuzzini, *Phys. Rev. Lett.* **89** (2002) 084101.
- [190] S. Wimberger Ph.D. thesis, Ludwig-Maximilians-Universität München and Università dell’Insubria Como, 2004, <http://edoc.ub.uni-muenchen.de/archive/00001687/>.
- [191] C. Müller, C. Miniatura, *J. Phys. A* **35** (2002) 10163.